

Model-Free Learning of Optimal Two-Stage Beamformers for Passive IRS-Aided Network Design

Hassaan Hashmi, *Student Member, IEEE*, Spyridon Pougkakiotis, and Dionysis Kalogerias, *Member, IEEE*

Abstract—Electronically tunable metasurfaces, or Intelligent Reflective Surfaces (IRSs), are a popular technology for achieving high spectral efficiency in modern wireless systems by shaping channels using a multitude of tunable passive reflective elements. Capitalizing on key practical limitations of IRS-aided beamforming pertaining to system modeling and channel sensing/estimation, we propose a novel, fully data-driven Zeroth-order Stochastic Gradient Ascent (ZoSGA) algorithm for general two-stage (i.e., short/long-term), fully-passive IRS-aided stochastic utility maximization. ZoSGA learns long-term optimal IRS beamformers jointly with short-term optimal precoders (e.g., WMMSE-based) via minimal zeroth-order reinforcement and in a strictly model-free fashion, relying solely on the *effective* compound channels observed at the terminals, while being independent of channel models or network/IRS configurations. Another remarkable feature of ZoSGA is being amenable to analysis, enabling us to establish a state-of-the-art (SOTA) convergence rate of the order of $\mathcal{O}(\sqrt{S}\epsilon^{-4})$ under minimal assumptions, where S is the total number of IRS elements, and ϵ is a desired suboptimality target. Our numerical results on a standard MISO downlink IRS-aided sumrate maximization setting establish SOTA empirical behavior of ZoSGA as well, consistently and substantially outperforming standard fully model-based baselines. Lastly, we demonstrate that ZoSGA can in fact operate *in the field*, by directly optimizing the capacitances of a varactor-based electromagnetic IRS model (unknown to ZoSGA) on a multiple user/IRS, compute-heavy network setting, with essentially no computational overheads or performance degradation.

Index Terms—6G, Intelligent Reflecting Surfaces (IRS/RIS), Two-stage Stochastic Programming, Zeroth-order Optimization, Model-Free Learning, Sumrate Maximization, Equivalent Circuit Model.

I. INTRODUCTION

The radical growth in the number of mobile and numerous other wireless devices, in particular those with communication modalities requiring high bandwidth and low latency connectivity such as virtual and augmented reality, tactile internet, internet of things, industrial automation, etc., have pushed existing wireless communication systems to their performance limits. The forthcoming era requires seamless wireless connectivity, necessitating proactive research beyond 5G communications [1]–[5].

Recently, 5G-enabling technologies such as mmWave communication, massive multi-input multi-output (MIMO) and dense networks have been vigorously investigated [6]–[9]. Still, deployment of both massive MIMO and dense networks incurs high installation/maintenance costs and energy consumption, while mmWaves exhibit physical limitations such as susceptibility to blockages and high propagation losses. To compensate for such propagation losses, which are a characteristic of higher carrier frequencies, densely packed and highly directional mmWave antennas have been proposed [10], [11]. High directionality, combined with reduced scattering, attenuates mmWave signals in

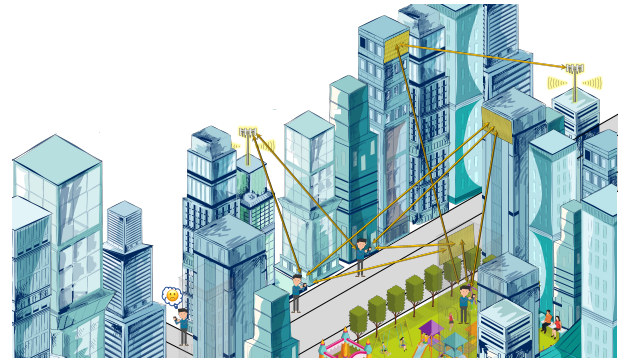


Fig. 1: Concept of an IRS-aided Wireless Network.

the non-line-of-sight (non-LOS) paths, thus blocking the signals. The reason lies in the physics of signal propagation: mmWaves exhibit a more prismatic propagation, i.e., they diffract less than microwave signals around obstacles [12].

Conventional beamforming, which is an established technique for improving Quality-of-Service (QoS) in wireless communications, cannot fully compensate for such non-LOS losses. One brute force solution would be to deploy ultra dense networks, i.e., networks with a large number of small cells, with service ranges of tens to hundreds of meters, allowing higher frequency reuse rates [13], [14]. With such low ranges, however, ultra-dense network deployment does not demonstrate economy of scale. Indeed, the consumption of energy increases sharply with the number of base stations. Additionally, such dense deployments would also exhibit acute signal interference patterns.

While the aforementioned approaches aim to improve QoS, they may fail to simultaneously satisfy the data-rate, bandwidth, latency, spectral and energy efficiency requirements of 5G-and-beyond technologies. This has necessitated efforts to develop innovative or even disruptive technologies that could meet such requirements, ideally without requiring extra energy and/or deployment or computational costs. An emerging technology for scalably reducing non-LOS losses while circumventing several limitations related to underlying propagation environments is that of *Intelligent Reflecting Surfaces (IRSs, or RISs)*. An IRS is a metasurface comprised of a planar array of passive reflective elements with tunable parameters, such as phase-shifts and/or amplitude gains of incident signals [15]–[19]. A concept network in which users (or terminals) are linked with an Access Point (AP) and enjoy improved QoS from the utilization of IRSs is shown in Figure 1.

In IRS-aided communications, the goal is to optimally tune the IRS elements along with other resources (such as AP precoders), so as to optimize a certain system utility. A standard setup is that of a weighted sumrate utility in a multi-user multiple-input single-output (MISO) downlink scenario, as depicted in Figure 1,

H. Hashmi, S. Pougkakiotis, and D. Kalogerias are with the Department of Electrical Engineering, Yale University, New Haven, CT, 06520 USA (email: {hassaan.hashmi, spyridon.pougkakiotis, dionysis.kalogerias}@yale.edu). This work is partially supported by a Microsoft gift.

where the goal is to maximize the total downlink rate of a number of users/terminals actively serviced by an AP, while *passively* aided by one or multiple IRSs [20]–[23]. For this standard setting, a core objective is to jointly optimize the IRS parameters and AP precoders under certain power constraints, noting that AP precoders are usually continuous-valued, while IRS phase-shifts can be either quantized [17], or continuously varying [18], [19].

Prior Art on IRS Optimization: Optimizing IRS parameters is a challenging task. In particular, there are three major bottlenecks. First, a sufficiently accurate channel model will most certainly be unknown, and even if known, it depends heavily on network structure and the surrounding environment. Second, by realistically assuming that IRSs are passive elements of the network, it might not be possible to continuously and reliably estimate the channel-state-information (CSI) of all intermediate channels, e.g., from APs to IRSs, and from IRSs to users/terminals [24], [25]; it is thus clear that IRS optimization should be free from the need of knowing such detailed CSI. Third, any reasonable IRS phase-shift tuning approach –which should only require *effective* CSI (i.e., the conventional compound channels observed at the corresponding end terminals)–, should also target as infrequent IRS parameter updates as possible, at least in long-term operation mode. This is in contrast with earlier approaches that consider fully reactive IRS infrastructure demanding resource-wasteful, perpetual IRS control [26], [27]. Addressing these challenges constitutes an active area of research. In fact, one or more of these bottlenecks are persistent in most of the proposed strategies for IRS optimization in wireless networks (see, e.g., [25], [28]).

Recently, model-based methods relying on some flavor of stochastic successive convex optimization (SSCO) [29]–[31] for weighted sumrate optimization have gained substantial traction. These methods operate over *two time-scale* customized protocols, where reactive precoding vectors at the AP(s) are optimized on a shorter time-scale and non-reactive (static, “long-term”) IRS beamformers are optimized on a longer time-scale [20]–[23]. Apart from relying on SSCO, which operates on convex surrogates of the original problem, these model-based approaches require complete knowledge of the network structure and the channel model, along with accurate intermediate CSI (statistic) estimation [32]–[35]. Such estimates are difficult to obtain because, as an ultimately passive device, an IRS cannot (or should not) transmit and receive pilot signals [24]. Consequently, these methods must rely on active sensing at the IRSs, demanding expensive and wasteful IRS implementations. Lastly, any change in the network or channel model incurs a high environment remodeling cost, while the modeling complexity increases dramatically with an increase in the number of intermediate channels.

To avoid such limitations, researchers have explored machine learning methods to optimize IRS-aided networks. As a parallel to channel estimation by hand, offline machine learning methods have been explored to approximate true CSI models from labelled datasets using function approximators (FAs) [36]–[39]. These offline approaches are brittle in that the learned models are unable to adapt to slight changes in the network/channel behavior, induced either by movement of the users/terminals, or due to potential environmental factors. Deep Reinforcement Learning (DRL) methods, on the other hand, are adaptive policy learning methods which have been used for joint beamforming

optimization. In particular, deep Q-learning based methods have been explored, assuming quantized IRS phase-shifts [40]–[43]. For continuous phase-shifts, off-policy policy gradient methods have also been explored [44]–[47], primarily based on the deep deterministic policy gradient (DDPG) algorithm [48]. DRL methods are designed to be *end-to-end*. As such, all intermediate steps such as CSI estimation, channel modeling and beamforming optimization can be *offloaded* to the FAs, the latter approximating state value functions to jointly model the entire optimization task.

Nonetheless, without expert domain knowledge, defining those FAs –e.g., deep neural networks (DNNs)– often increases the problem complexity; most frequently, FAs are considered as black-box data-driven models, resulting in non-interpretability and lack of robustness. On the other hand, explicit utilization of domain knowledge within the context of FAs often results in overfitting, thus limiting the versatility and transferability of DRL models to distinct environments. Further, such learning-based methods incur increased power/resource consumption as they primarily consider reactive IRS operation, where each model output (phase-shift element values) directly depends on the observed CSI, hence resulting in perpetual IRS control. Combinations of the mixed-timescale iterative approach with machine learning via deep unfolding models [49] also suffer from similar limitations.

Contributions: We develop a *Zeroth-order Stochastic Gradient Ascent (ZoSGA)* algorithm suitable for tackling general two-stage stochastic programming, specifically suitable for *fully passive* IRS-assisted utility maximization in a wireless setting. As discussed in Section II, the first-stage problem consists of an on-average (long-term) optimization of IRS-parameters, while the second-stage problem seeks for optimal instantaneous (short-term) beamformers (e.g., of an AP) associated with a given network instance (occurring every time new –random– CSI is revealed). ZoSGA tacitly exploits WMMSE [50] as a standard method for solving the (deterministic) second-stage problems, while remaining agnostic to the channel dynamics or network topology, thus operating in a completely model-free manner. The algorithm relies on minimal system probing and terminal-end effective CSI, both conventionally available (even approximately) regardless of the number or spatial configuration of the IRSs, in sharp contrast to model-based approaches [20]–[23].

ZoSGA does not rely on function approximations (unlike DRL methods [40]–[47]), and can be run in real-time since, at each time step, it only requires to probe the network twice (to obtain a sample zeroth-order gradient), greatly improving upon SSCO-based methods, such as TTS-SSCO [21], which utilize internal (model-based) sampling for approximating stochastic gradients. Assuming continuous-valued IRS phase-shifts (feasible in practice [18], [19]), ZoSGA treats IRSs as fully passive tunable network elements (without sensing capabilities, extra hardware, or special scheduling requirements), and can be readily applied to a wide range of different wireless network settings.

After developing some preliminary technical results (Section III), we develop and analyze ZoSGA (Section IV) under two distinct sets of minimal assumptions (and regularity conditions), and we establish a state-of-the-art (SOTA) convergence rate of the order of $\mathcal{O}(\sqrt{S}\epsilon^{-4})$, where S is the total number of IRS tunable parameters and ϵ is a desirable sub-optimality target. The first set of assumptions requires an oracle yielding global solutions

to the second-stage problems (e.g., optimal AP precoding). We note that this is a standard assumption in the literature of two-stage stochastic programming (e.g. see [51]). While this technical framework is powerful and important in its own right (e.g., it allows us to show that ZoSGA obtains locally optimal solutions), it does not capture most practical settings, in which we can only hope for stationary points from the application of WMMSE. To deal with this case, we introduce a second set of assumptions under which ZoSGA obtains a local optimum of a related (approximating) problem. The quality of this related problem depends on that of the stationary points obtained by WMMSE (or any method providing such solutions). Our analysis covers a wide range of realistic settings and sheds light into the practical behavior of ZoSGA, also fully characterizing its convergence.

Specializing to the case of sumrate maximization on a MISO downlink scenario (Section V), we show that most of the technical assumptions imposed by the theory are automatically satisfied, except for some mild regularity conditions on the channel which cannot be avoided. We then numerically demonstrate (Section VI) that ZoSGA exhibits SOTA performance in a wide-range of scenarios, substantially outperforming the two-time scale method recently proposed in [21], which is a standard *model-based* SSCO-type SOTA baseline for the problem under consideration. Despite the latter method assuming full knowledge of channel models and spatial network configurations, the model-agnostic ZoSGA reliably learns near-optimal solutions yielding significantly better QoS. Importantly, we also demonstrate the applicability of ZoSGA in a realistic *physical* IRS setting, in which the algorithm has only *indirect access* to the amplitudes and phases of the IRS elements, by tuning the capacitances of certain varactor diodes controlling each IRS element; such IRS tuning *in the field* is a particularly unique feature of ZoSGA, not enjoyed by any other IRS tuning approach in the literature. Fully reproducible source code of simulation results can be found [here](#).

Notation: Let $\|\cdot\|$ denote the induced norm of an associated inner-product space, defined as $\|\mathbf{x}\| := \sqrt{\langle \mathbf{x}, \mathbf{x} \rangle}$ for any $\mathbf{x} \in \mathbb{F}^n$, where \mathbb{F} is a field (assuming that $\mathbb{F} = \mathbb{R}$ or $\mathbb{F} = \mathbb{C}$). In case of a complex vector we use the Hermitian inner product. In case of a matrix we assume that the induced norm is utilized. We assume a complete base probability space (Ξ, \mathcal{F}, P) , and use “a.e.” to denote “almost every(where)”. For $p \in [1, \infty)$, we use $\mathcal{Z}_p \equiv \mathcal{L}_p(\Xi, \mathcal{F}, P; \mathbb{R})$ to denote the space of all \mathcal{F} -measurable functions $\phi: \Xi \rightarrow \mathbb{R}$, such that $\int_{\Xi} |\phi|^p dP < \infty$.

II. PROBLEM FORMULATION

In an IRS-aided network, the effective channels observed at the terminals of the communication task are treated as functions of both the intermediate channels as well the phase-shift vectors of the IRSs. Thus, we may think of the IRSs as *network-defining* parameters. Indeed, each instance of their phase-shift elements produces a different wireless network altogether. Taking this into account, the objective here is to find an optimal instance of such a wireless network which maximizes a given terminal QoS utility, in accordance with all the underlying physical dynamics.

Traditionally, we only optimize the precoding vectors (e.g., at an AP) to maximize a given QoS metric function, and these precoding vectors are optimized for a particular wireless network instance. However, in an IRS-aided wireless network, tuning the

IRSs essentially changes the network structure and we have to re-optimize the precoders, responding to this new network.

We assume dynamic (i.e. reactive) precoders \mathbf{W} , while (realistically) viewing the IRSs as static (i.e. non-reactive during operation) elements with tunable parameters $\boldsymbol{\theta}$ (such as in [20]–[23]), which encode any propagation feature of the IRSs that is learnable. For example, $\boldsymbol{\theta}$ can represent amplitudes and/or phases, or any other tunable element of an IRS (e.g., *physical* varactor tunable capacitances, see [18], [19]).

Under this setting, beamforming optimization can be formulated as a *stochastic two-stage problem*. The first-stage problem seeks for an optimal (say in expectation) wireless network by tuning the (static) IRSs parameters $\boldsymbol{\theta}$ assuming optimal instantaneous precoders on random effective channels. The second-stage problem seeks those optimal precoders \mathbf{W} given a (possibly optimal) network instance set by already fixing the IRSs.

We hereafter assume that the IRSs and the precoders maximize the same QoS utility function. This is an intuitive and standard choice in practical applications, which enables the development of very efficient solution methods. Formally, we are interested in two-stage problems of the form

$$\max_{\boldsymbol{\theta} \in \Theta} \mathbb{E} \left\{ \max_{\mathbf{W} \in \mathcal{W}} F(\mathbf{W}, \mathbf{H}(\boldsymbol{\theta}, \omega)) \right\}, \quad (2SP)$$

where \mathcal{W} is a compact set for the dynamic beamformers \mathbf{W} , and $\Theta \subset \mathbb{R}^S$ is a convex and compact set of feasible IRS parameter values. The utility function $F: \mathbb{C}^M \times \mathbb{C}^M \rightarrow \mathbb{R}$ is a function of the precoding vectors \mathbf{W} as well as the observed effective channels $\mathbf{H}: \Theta \times \Omega \rightarrow \mathbb{C}^M$, which in turn are functions of both the IRS phase-shift elements and any intermediate random channels (a “state of nature”), denoted as $\omega: \Xi \rightarrow \Omega$ (the statistics of which are unknown).

As we discuss in Section III-C, the resulting stochastic bilevel program assumes a common function for the inner- and outer-level programs, allowing for first-order optimization, without the need of computing any second-order information (e.g. as in [51]).

III. PRELIMINARIES AND TECHNICAL RESULTS

A. Problem Description and Assumptions

In what follows, we provide certain regularity assumptions on (2SP) and subsequently prove certain core technical results, allowing us to derive the proposed optimization scheme.

Second-stage problem: Given some realization $\omega \in \Omega$, and some $\boldsymbol{\theta} \in \Theta$, the second-stage problem reads

$$\max_{\mathbf{W} \in \mathcal{W}} \{G(\mathbf{W}, \boldsymbol{\theta}, \omega) \triangleq F(\mathbf{W}, \mathbf{H}(\boldsymbol{\theta}, \omega))\}. \quad (SSP)$$

Notice that (SSP) is deterministic, since we are required to solve this after the state of nature ω has been revealed.

First-stage problem: The first-stage problem, which is equivalently given in (2SP), can be provisionally written as

$$\max_{\boldsymbol{\theta} \in \Theta} \{f(\boldsymbol{\theta}) \triangleq \mathbb{E} \{F(\mathbf{W}^*(\boldsymbol{\theta}, \omega), \mathbf{H}(\boldsymbol{\theta}, \omega))\}\} \quad (FSP)$$

for some $\mathbf{W}^*(\boldsymbol{\theta}, \omega) \in \arg \max_{\mathbf{W} \in \mathcal{W}} F(\mathbf{W}, \mathbf{H}(\boldsymbol{\theta}, \omega))$. In what follows, we enforce certain regularity conditions on (2SP).

Assumption A. The following conditions are in effect:

(A1) The function $F: \mathbb{C}^M \times \mathbb{C}^M \rightarrow \mathbb{R}$ is twice continuously (real) differentiable;

- (A2) The sets Θ and \mathcal{W} are compact, and Θ is also convex;
- (A3) The function $\mathbf{H}(\cdot, \omega)$ is B_H -uniformly bounded on Θ and twice continuously differentiable on an open set $\mathcal{U} \supset \Theta$, for a.e. $\omega \in \Omega$. Moreover, there exist numbers $L_{H,0}$, $L_{H,1}$, such that $\mathbf{H}(\cdot, \omega)$ is $L_{H,0}$ -Lipschitz continuous with $L_{H,1}$ -Lipschitz gradients on Θ for a.e. $\omega \in \Omega$;
- (A4) For a.e. $\omega \in \Omega$ and all $\theta \in \Theta$, the partial (real) Hessian $\frac{\partial^2}{\partial \mathbf{W}^2} F(\mathbf{W}, \mathbf{H}(\theta, \omega)) \Big|_{\mathbf{W}=\mathbf{W}^*(\theta, \omega)}$ is nonsingular for any $\mathbf{W} = \mathbf{W}^*(\theta, \omega) \in \arg \max_{\mathbf{W} \in \mathcal{W}} F(\mathbf{W}, \mathbf{H}(\theta, \omega))$;
- (A5) $F(\mathbf{W}^*(\theta, \cdot), \mathbf{H}(\theta, \cdot)) \in \mathcal{Z}_2$ is bounded below for all $\theta \in \Theta$ and some $\mathbf{W}^*(\theta, \omega) \in \arg \max_{\mathbf{W} \in \mathcal{W}} F(\mathbf{W}, \mathbf{H}(\theta, \omega))$, and we can draw independent and identically distributed (i.i.d.) samples from the law of ω .

Remark 1. Conditions (A1)–(A2) are standard and are most often met in practical settings. Note that *real differentiability* refers to differentiability of the real and imaginary parts of F (see [52, Section 3.2]). Condition (A3) ensures that the compositional function of interest is well-defined and retains its properties on an open set containing Θ , while the bound and Lipschitz random functions of $\mathbf{H}(\cdot, \omega)$ are uniformly bounded in ω . The latter condition could potentially be relaxed (e.g. assuming bounded variance of random functions $B_{H,0}(\omega)$, $L_{H,0}(\omega)$, $L_{H,1}(\omega)$), but is imposed for brevity in exposition. (A4) is a technical condition imposing regularity on (2SP). In particular, it ensures that the solution mapping $\mathbf{W} \mapsto \arg \max_{\mathbf{W} \in \mathcal{W}} F(\mathbf{W}, \mathbf{H}(\theta, \omega))$ has a single-valued *localization* around each $\mathbf{W}^*(\theta, \omega)$ (via the implicit function theorem [53]), which in turn ensures that $\mathbf{W}^*(\cdot, \omega)$ is locally continuously differentiable. As we discuss later, this condition can be enforced by appropriately regularizing the problem. Also, note that this condition refers to the real partial Hessian (i.e., with respect to the real- and imaginary-parts of $F(\cdot, \mathbf{H})$; see [52, Section 6.2]). Finally, condition (A5) ensures that f is well-defined and bounded on Θ . Notice that the same would hold under the weaker condition $F(\mathbf{W}^*(\theta, \cdot), \mathbf{H}(\theta, \cdot)) \in \mathcal{Z}_1$, however (A5) is utilized later in Lemma 6.

B. The Gradient of the Second-Stage Objective Function

In light of conditions (A1)–(A3) of Assumption A, we can easily show that $F(\mathbf{W}, \mathbf{H}(\theta, \omega))$ (i.e., the objective function in (SSP)) admits an explicit usual (Fréchet) gradient, for all $\theta \in \mathcal{U}$ and a.e. $\omega \in \Omega$. We do this by utilizing elements of *Wirtinger calculus* (see [52, Section 4] for a detailed exposition).

Indeed, in order to evaluate the gradient of $F(\mathbf{W}, \mathbf{H}(\cdot, \omega))$, i.e., $\nabla_{\theta} F(\mathbf{W}, \mathbf{H}(\cdot, \omega)) : \mathcal{U} \rightarrow \mathbb{R}^S$, we consider its *Wirtinger cogradient* (a row vector; see [52, Section 4.2]), defined as

$$\frac{\partial^{\circ}}{\partial \mathbf{z}} F(\mathbf{W}, \mathbf{H}(\mathbf{z}, \omega)) \triangleq \frac{1}{2} \left(\frac{\partial}{\partial \Re(\mathbf{z})} F(\mathbf{W}, \mathbf{H}(\mathbf{z}, \omega)) - j \frac{\partial}{\partial \Im(\mathbf{z})} F(\mathbf{W}, \mathbf{H}(\mathbf{z}, \omega)) \right),$$

noting that $\mathbf{H}(\mathbf{z}, \omega)$ is constant relative to $\Im(\mathbf{z})$, i.e.

$$\mathbf{H}(\mathbf{z}, \omega) = \mathbf{H}(\mathbf{x} + j\mathbf{y}, \omega) = \mathbf{H}(\mathbf{x}, \omega), \quad \forall (\mathbf{x}, \mathbf{y}) \in \mathcal{U} \times \mathcal{U},$$

and hence so is $F(\mathbf{W}, \mathbf{H}(\mathbf{z}, \omega))$. It then follows that

$$\frac{\partial^{\circ}}{\partial \mathbf{z}} F(\mathbf{W}, \mathbf{H}(\mathbf{z}, \omega)) = \frac{1}{2} (\nabla_{\mathbf{x}} F(\mathbf{W}, \mathbf{H}(\mathbf{x}, \omega)))^{\top}.$$

Using the Wirtinger chain rule (see [52, Eq. (32)]), we obtain

$$\begin{aligned} \frac{\partial^{\circ}}{\partial \mathbf{z}} F(\mathbf{W}, \mathbf{H}(\mathbf{z}, \omega)) &= \frac{\partial^{\circ}}{\partial \mathbf{z}} F(\mathbf{W}, \mathbf{z}) \Big|_{\mathbf{z}=\mathbf{H}(\mathbf{x}, \omega)} \frac{\partial^{\circ}}{\partial \mathbf{z}} \mathbf{H}(\mathbf{z}, \omega) \\ &\quad + \frac{\partial^{\circ}}{\partial \bar{\mathbf{z}}} F(\mathbf{W}, \mathbf{z}) \Big|_{\mathbf{z}=\mathbf{H}(\mathbf{x}, \omega)} \frac{\partial^{\circ}}{\partial \bar{\mathbf{z}}} \overline{\mathbf{H}(\mathbf{z}, \omega)}, \end{aligned}$$

where $\bar{\mathbf{z}}$ denotes the complex conjugate of \mathbf{z} . It follows that

$$\begin{aligned} \frac{\partial^{\circ}}{\partial \mathbf{z}} \mathbf{H}(\mathbf{z}, \omega) &= \frac{1}{2} \left(\frac{\partial}{\partial \Re(\mathbf{z})} \mathbf{H}(\mathbf{z}, \omega) - j \frac{\partial}{\partial \Im(\mathbf{z})} \mathbf{H}(\mathbf{z}, \omega) \right) \\ &= \frac{1}{2} \left((\nabla_{\mathbf{x}} \Re(\mathbf{H}(\mathbf{x}, \omega)))^{\top} + j (\nabla_{\mathbf{x}} \Im(\mathbf{H}(\mathbf{x}, \omega)))^{\top} \right), \end{aligned}$$

and

$$\frac{\partial^{\circ}}{\partial \bar{\mathbf{z}}} \overline{\mathbf{H}(\mathbf{z}, \omega)} = \overline{\left(\frac{\partial^{\circ}}{\partial \mathbf{z}} \mathbf{H}(\mathbf{z}, \omega) \right)}.$$

From the real-valuedness of $F(\mathbf{W}, \mathbf{H}(\cdot, \omega))$, we have

$$\begin{aligned} \frac{\partial^{\circ}}{\partial \mathbf{z}} F(\mathbf{W}, \mathbf{H}(\mathbf{x}, \omega)) &= \frac{\partial^{\circ}}{\partial \mathbf{z}} F(\mathbf{W}, \mathbf{z}) \Big|_{\mathbf{z}=\mathbf{H}(\mathbf{x}, \omega)} \frac{\partial^{\circ}}{\partial \mathbf{z}} \mathbf{H}(\mathbf{z}, \omega) \\ &\quad + \overline{\left(\frac{\partial^{\circ}}{\partial \mathbf{z}} F(\mathbf{W}, \mathbf{z}) \Big|_{\mathbf{z}=\mathbf{H}(\mathbf{x}, \omega)} \frac{\partial^{\circ}}{\partial \bar{\mathbf{z}}} \overline{\mathbf{H}(\mathbf{z}, \omega)} \right)} \\ &= 2\Re \left(\frac{\partial^{\circ}}{\partial \mathbf{z}} F(\mathbf{W}, \mathbf{z}) \Big|_{\mathbf{z}=\mathbf{H}(\mathbf{x}, \omega)} \frac{\partial^{\circ}}{\partial \mathbf{z}} \mathbf{H}(\mathbf{z}, \omega) \right). \end{aligned}$$

Thus, for any $\theta \in \mathcal{U}$ and a.e. $\omega \in \Omega$, we obtain

$$\begin{aligned} \nabla_{\theta} F(\mathbf{W}, \mathbf{H}(\theta, \omega)) &= 2\nabla_{\theta} \Re(\mathbf{H}(\theta, \omega)) \Re \left(\frac{\partial^{\circ}}{\partial \mathbf{z}} F(\mathbf{W}, \mathbf{z}) \Big|_{\mathbf{z}=\mathbf{H}(\theta, \omega)} \right)^{\top} \\ &\quad + 2\nabla_{\theta} \Im(\mathbf{H}(\theta, \omega)) \Re \left(j \frac{\partial^{\circ}}{\partial \mathbf{z}} F(\mathbf{W}, \mathbf{z}) \Big|_{\mathbf{z}=\mathbf{H}(\theta, \omega)} \right)^{\top}. \end{aligned} \quad (1)$$

C. Technical Results

We proceed by proving that for a.e. $\omega \in \Omega$, the Wirtinger gradient of F , evaluated at some $\mathbf{z} = \mathbf{H}(\theta, \omega)$, for any $\theta \in \Theta$, is bounded by a positive constant, independent of ω .

Lemma 1. *Given Assumption A, there exists a constant $B_F > 0$ such that, for all $(\theta, \mathbf{W}) \in \Theta \times \mathcal{W}$, and a.e. $\omega \in \Omega$,*

$$\left\| \frac{\partial^{\circ}}{\partial \mathbf{z}} F(\mathbf{W}, \mathbf{z}) \Big|_{\mathbf{z}=\mathbf{H}(\theta, \omega)} \right\| \leq B_F.$$

Proof. From (A3) we obtain that the sets $\mathbf{H}(\Theta, \omega)$, for $\omega \in \Omega$, are uniformly (in ω) compact. Thus, we can find a compact set \mathcal{V} , such that $\mathbf{H}(\Theta, \omega) \subset \mathcal{V}$ for a.e. $\omega \in \Omega$. From (A2) we also have that \mathcal{W} compact. Since F is continuously (real) differentiable on the compact set $\mathcal{V} \times \mathcal{W}$, it follows from the extreme value theorem applied to $\frac{\partial}{\partial \Re(\mathbf{z})} F(\mathbf{W}, \mathbf{z})$ and to $\frac{\partial}{\partial \Im(\mathbf{z})} F(\mathbf{W}, \mathbf{z})$, respectively, with $\mathbf{z} \in \mathcal{V}$, that there exists some constant B_F such that

$$\left\| \frac{\partial}{\partial \Re(\mathbf{z})} F(\mathbf{W}, \mathbf{z}) \Big|_{\mathbf{z}=\mathbf{H}(\theta, \omega)} \right\| \leq B_F,$$

$$\left\| \frac{\partial}{\partial \mathfrak{S}(z)} F(\mathbf{W}, z) \Big|_{z=\mathbf{H}(\boldsymbol{\theta}, \omega)} \right\| \leq B_F,$$

for a.e. $\omega \in \Omega$ and any $(\boldsymbol{\theta}, \mathbf{W}) \in \Theta \times \mathcal{W}$. To complete the proof, we simply bound the Wirtinger cogradient directly by its definition (adjusting the constant upper bound). \square

We now state the *implicit function theorem*, specialized in the case of problem (FSP)–(SSP). This will later on be utilized to show that in fact the objective of (FSP) is differentiable on Θ .

Theorem 2 (Implicit Function Theorem). *Let Assumption A be in effect. For every $\boldsymbol{\theta}_\circ \in \Theta$, $\mathbf{W}^* \in \arg \max_{\mathbf{W} \in \mathcal{W}} G(\mathbf{W}, \boldsymbol{\theta}_\circ, \omega)$, and a.e. $\omega \in \Omega$, there exists an open neighbourhood Θ_\circ of $\boldsymbol{\theta}_\circ$ on which there exists a unique continuously differentiable (implicit) mapping $\mathbf{W}_\circ^*(\cdot, \omega): \boldsymbol{\theta} \mapsto \arg \max_{\mathbf{W} \in \mathcal{W}} G(\mathbf{W}, \boldsymbol{\theta}, \omega)$, for all $\boldsymbol{\theta} \in \Theta_\circ$, satisfying $\mathbf{W}_\circ^*(\boldsymbol{\theta}_\circ, \omega) = \mathbf{W}^*$. Moreover, for any $\boldsymbol{\theta} \in \Theta_\circ$,*

$$\frac{\partial}{\partial \boldsymbol{\theta}} \mathbf{W}_\circ^*(\boldsymbol{\theta}, \omega) = -M \frac{\partial^2}{\partial \boldsymbol{\theta} \partial \mathbf{W}} F(\mathbf{W}_\circ^*(\boldsymbol{\theta}, \omega), \mathbf{H}(\boldsymbol{\theta}, \omega)),$$

where $M \equiv M(\mathbf{W}_\circ^*, \boldsymbol{\theta}, \omega)$ and

$$M(\mathbf{W}_\circ^*, \boldsymbol{\theta}, \omega) \triangleq \left(\frac{\partial^2}{\partial \mathbf{W}^2} F(\mathbf{W}, \mathbf{H}(\boldsymbol{\theta}, \omega)) \Big|_{\mathbf{W}=\mathbf{W}_\circ^*(\boldsymbol{\theta}, \omega)} \right)^{-1}.$$

Proof. This is the standard implicit function theorem (e.g. see [53, Theorem 1B.1]), specialized to problem (2SP). It follows from conditions (A1)–(A4) of Assumption A. Note that by condition (A4) the matrix $M(\mathbf{W}_\circ^*, \boldsymbol{\theta}, \omega)$ is nonsingular. \square

Theorem 2 and condition (A5) allow us to show that the objective of (FSP) is differentiable for any $\boldsymbol{\theta} \in \Theta$ and $\mathbf{W}^* \equiv \mathbf{W}^*(\boldsymbol{\theta}, \omega) \in \arg \max_{\mathbf{W} \in \mathcal{W}} G(\mathbf{W}, \boldsymbol{\theta}, \omega)$. To see this, we first provide a generalization of *Danskin's theorem* (see [54] for a standard version of this result), which follows as a consequence of Theorem 2.

Corollary 3. *Let Assumption A hold. Then, for a.e. $\omega \in \Omega$, any $\boldsymbol{\theta} \in \Theta$, and any $\mathbf{W}^*(\boldsymbol{\theta}, \omega) \in \arg \max_{\mathbf{W} \in \mathcal{W}} G(\mathbf{W}, \boldsymbol{\theta}, \omega)$, the function $F(\mathbf{W}^*(\boldsymbol{\theta}, \omega), \boldsymbol{\theta}, \omega)$ is differentiable at $\boldsymbol{\theta}$, and*

$$\begin{aligned} \nabla_{\boldsymbol{\theta}} F(\mathbf{W}^*(\boldsymbol{\theta}, \omega), \mathbf{H}(\boldsymbol{\theta}, \omega)) \\ = \nabla_{\boldsymbol{\theta}} F(\mathbf{W}, \mathbf{H}(\boldsymbol{\theta}, \omega)) \Big|_{\mathbf{W}=\mathbf{W}^*(\boldsymbol{\theta}, \omega)}. \end{aligned} \quad (2)$$

Proof. Let us fix any $\boldsymbol{\theta} \in \Theta$, and for a.e. $\omega \in \Omega$, fix an arbitrary element $\mathbf{W}^*(\boldsymbol{\theta}, \omega) \in \arg \max_{\mathbf{W} \in \mathcal{W}} G(\mathbf{W}, \boldsymbol{\theta}, \omega)$. Then, we can invoke Theorem 2 to deduce the existence of a unique and continuously differentiable implicit function $\mathbf{W}_\circ^*(\cdot, \omega)$ on an open neighbourhood Θ_\circ of $\boldsymbol{\theta}$, with $\mathbf{W}_\circ^*(\boldsymbol{\theta}, \omega) = \mathbf{W}^*(\boldsymbol{\theta}, \omega)$. In particular, for any $\boldsymbol{\theta} \in \Theta_\circ$, we can use the chain rule to obtain

$$\begin{aligned} \nabla_{\boldsymbol{\theta}} F(\mathbf{W}_\circ^*(\boldsymbol{\theta}, \omega), \mathbf{H}(\boldsymbol{\theta}, \omega)) \\ = \nabla_{\boldsymbol{\theta}} F(\mathbf{W}, \mathbf{H}(\boldsymbol{\theta}, \omega)) \Big|_{\mathbf{W}=\mathbf{W}_\circ^*(\boldsymbol{\theta}, \omega)} \\ + \nabla_{\mathbf{W}} F(\mathbf{W}_\circ^*(\boldsymbol{\theta}, \omega), \mathbf{H}(\boldsymbol{\theta}, \omega)) \frac{\partial}{\partial \boldsymbol{\theta}} \mathbf{W}_\circ^*(\boldsymbol{\theta}, \omega). \end{aligned}$$

Upon noting that $\nabla_{\mathbf{W}} F(\mathbf{W}^*(\boldsymbol{\theta}, \omega), \mathbf{H}(\boldsymbol{\theta}, \omega)) = \mathbf{0}$ (by construction), $\mathbf{W}_\circ^*(\boldsymbol{\theta}, \omega) = \mathbf{W}^*(\boldsymbol{\theta}, \omega)$, while $\frac{\partial}{\partial \boldsymbol{\theta}} \mathbf{W}_\circ^*(\boldsymbol{\theta}, \omega)$ is well-defined and bounded, the result follows. \square

Theorem 4. *Let Assumption A hold. Then, for a.e. $\omega \in \Omega$, there exists a bounded constant $L_{F,1}(\omega) > 0$, such that the function $F(\mathbf{W}^*(\cdot, \omega), \mathbf{H}(\cdot, \omega)): \Theta \rightarrow \mathbb{R}$ is $L_{F,1}(\omega)$ -Lipschitz smooth on Θ , where $\mathbf{W}^*(\boldsymbol{\theta}, \omega)$ is an arbitrary selection of*

$\arg \max_{\mathbf{W} \in \mathcal{W}} G(\mathbf{W}, \boldsymbol{\theta}, \omega)$. Moreover, $-F(\mathbf{W}^*(\cdot, \omega), \mathbf{H}(\cdot, \omega))$ is $L_{F,1}(\omega)$ -weakly convex on Θ .

Proof. Consider the function $\nabla_{\boldsymbol{\theta}} F(\mathbf{W}^*(\cdot, \omega), \mathbf{H}(\cdot, \omega)): \Theta \rightarrow \mathbb{R}^n$. We first note that its domain (i.e. Θ) is compact. Additionally, for a.e. $\omega \in \Omega$, we invoke Theorem 2 and Corollary 3 to obtain that the function is continuously differentiable at any $\boldsymbol{\theta} \in \Theta$. These two conditions imply that it is in fact $L_{F,1}(\omega)$ -Lipschitz continuous on Θ , for some Lipschitz constant $L_{F,1}(\omega) > 0$. The proof is complete upon noticing that Lipschitz smoothness implies weak convexity (with the same constant; see [55]). \square

We are now ready to show that f in (FSP) is actually differentiable on Θ , while under the mild assumption of integrability of $L_{F,1}(\omega)$ (given in Theorem 4), that it is also weakly convex.

Theorem 5. *Let Assumption A hold. Then, for any $\boldsymbol{\theta} \in \Theta$, the function f is well-defined and differentiable, with*

$$\nabla_{\boldsymbol{\theta}} f(\boldsymbol{\theta}) = \mathbb{E} \left\{ \nabla_{\boldsymbol{\theta}} F(\mathbf{W}, \mathbf{H}(\boldsymbol{\theta}, \omega)) \Big|_{\mathbf{W}=\mathbf{W}^*(\boldsymbol{\theta}, \omega)} \right\}, \quad (3)$$

for any $\mathbf{W}^*(\boldsymbol{\theta}, \omega) \in \arg \max_{\mathbf{W} \in \mathcal{W}} F(\mathbf{W}, \mathbf{H}(\boldsymbol{\theta}, \omega))$. Moreover, if $L_{F,1}(\cdot) \in \mathcal{Z}_1$, where $L_{F,1}(\omega)$ is given in Theorem 4, then there exists a positive constant $\rho \triangleq \mathbb{E}\{L_{F,1}(\omega)\}$, such that f is ρ -weakly convex on Θ .

Proof. Condition (A5) ensures that f is well-defined and bounded for any $\boldsymbol{\theta} \in \Theta$. Using Corollary 3 and [56, Theorem 7.44], the gradient of f exists for all $\boldsymbol{\theta} \in \Theta$, and reads

$$\nabla_{\boldsymbol{\theta}} f(\boldsymbol{\theta}) = \mathbb{E} \left\{ \nabla_{\boldsymbol{\theta}} F(\mathbf{W}, \mathbf{H}(\boldsymbol{\theta}, \omega)) \Big|_{\mathbf{W}=\mathbf{W}^*(\boldsymbol{\theta}, \omega)} \right\},$$

where $\mathbf{W}^*(\boldsymbol{\theta}, \cdot) \in \arg \max_{\mathbf{W} \in \mathcal{W}} F(\mathbf{W}, \mathbf{H}(\boldsymbol{\theta}, \cdot))$ is an arbitrary selection. Under the additional assumption of integrability of $L_{F,1}(\omega)$, ρ -weak convexity of f follows from Theorem 4. \square

Remark 2. Let us observe that the integrability assumption of the Lipschitz smooth constants $L_{F,1}(\omega)$ (arising from Theorem 4) is very mild and is almost always met in practice (where one usually has a finite collection of scenarios). As such, for the rest of this article we make the implicit assumption that this holds.

D. Zeroth-order Gradient Approximation of the Channel

Assuming the lack of availability of any first-order information of $\mathbf{H}(\cdot, \omega)$ for any $\omega \in \Omega$, we will employ a zeroth-order scheme in order to obtain a gradient estimate of $\nabla_{\boldsymbol{\theta}} \mathbf{H}(\cdot, \omega)$, using which we can solve (FSP) via a stochastic projected gradient ascent scheme. The proposed method will be based on gradient estimates arising from a two-point stochastic evaluation of $\mathbf{H}(\cdot, \omega)$ (similar to, among others, [57]–[59]). From (A3), we have

$$\nabla_{\boldsymbol{\theta}} \mathbf{H}(\boldsymbol{\theta}, \omega) = \nabla_{\boldsymbol{\theta}} \Re(\mathbf{H}(\boldsymbol{\theta}, \omega)) + j \nabla_{\boldsymbol{\theta}} \Im(\mathbf{H}(\boldsymbol{\theta}, \omega)).$$

We would like to approximate each of the above parts of the gradient using only function evaluations of $\mathbf{H}(\cdot, \omega)$. We let $\mathbf{U} \sim \mathcal{N}(\mathbf{0}, \mathbf{I})$ be a normal random vector, where \mathbf{I} is the identity matrix of size S . Given a smoothing parameter $\mu > 0$, we consider the following gradient estimate

$$\begin{aligned} \nabla_{\boldsymbol{\theta}} \mathbf{H}_\mu(\boldsymbol{\theta}, \omega) &\triangleq \frac{1}{2\mu} \mathbb{E} \left\{ (\mathbf{H}(\boldsymbol{\theta} + \mu \mathbf{U}, \omega) - \mathbf{H}(\boldsymbol{\theta} - \mu \mathbf{U}, \omega)) \mathbf{U}^\top \right\}^\top \\ &\equiv \nabla_{\boldsymbol{\theta}} \mathbf{H}_\mu^R(\boldsymbol{\theta}, \omega) + j \nabla_{\boldsymbol{\theta}} \mathbf{H}_\mu^I(\boldsymbol{\theta}, \omega), \end{aligned} \quad (4)$$

where $\nabla_{\theta} \mathbf{H}_{\mu}^R(\theta, \omega) \triangleq \Re(\nabla_{\theta} \mathbf{H}_{\mu}(\theta, \omega))$ and $\nabla_{\theta} \mathbf{H}_{\mu}^I(\theta, \omega) \triangleq \Im(\nabla_{\theta} \mathbf{H}_{\mu}(\theta, \omega))$. Let us notice that given condition **(A3)**, there exists an open set $\mathcal{U} \supset \Theta$ such that (4) is still well-defined. Thus, the gradient approximation is valid, even if θ is a point in the boundary of Θ , assuming that an appropriately small μ is chosen. Observe that the smaller the value of μ is, the better the aforementioned zeroth-order approximation is. There is a trade-off between approximation accuracy and numerical stability, but in practice we observe that μ can be chosen to be quite small.

The proposed zeroth-order gradient approximation of (1), based on the zeroth-order approximation given in (4), reads

$$\begin{aligned} & \nabla_{\theta}^{\mu} F(\mathbf{W}, \mathbf{H}(\theta, \omega)) \\ & \triangleq 2\nabla_{\theta} \mathbf{H}_{\mu}^R(\theta, \omega) \left(\Re \left(\frac{\partial^{\circ}}{\partial \mathbf{z}} F(\mathbf{W}, \mathbf{z}) \Big|_{\mathbf{z}=\mathbf{H}(\theta, \omega)} \right) \right)^{\top} \\ & \quad + 2\nabla_{\theta} \mathbf{H}_{\mu}^I(\theta, \omega) \left(\Re \left(j \frac{\partial^{\circ}}{\partial \mathbf{z}} F(\mathbf{W}, \mathbf{z}) \Big|_{\mathbf{z}=\mathbf{H}(\theta, \omega)} \right) \right)^{\top}, \end{aligned} \quad (5)$$

where $\mathbf{H}_{\mu}^R(\theta, \omega)$ and $\mathbf{H}_{\mu}^I(\theta, \omega)$ are given in (4).

E. An Approximate Problem Formulation

Let us notice that the analysis in the previous subsections assumed the availability of a globally optimal solution to the deterministic second-stage problem **(SSP)**. However, in the non-convex case, such an assumption might be unrealistically strong. Instead, in practice one usually hopes for a locally optimal solution, via identifying a stationary point of the inner problem. In other words, practical algorithms often solve an approximation of **(FSP)**, of the following form

$$\max_{\theta \in \Theta} \{f(\theta) \triangleq \mathbb{E}\{F(\mathbf{W}^{\circ}(\theta, \omega), \mathbf{H}(\theta, \omega))\}\}, \quad (\text{FSP}')$$

where $\mathbf{W}^{\circ}(\theta, \omega) \in \{\mathbf{W} \in \mathcal{W} \mid \frac{\partial}{\partial \mathbf{W}} F(\mathbf{W}, \mathbf{H}(\theta, \omega)) = \mathbf{0}\}^1$.

Solving **(FSP')** does not guarantee optimal solutions to **(FSP)**, but only approximate ones. Nonetheless, it is a standard approximation employed in practice. At this point, we can observe that all of the previously stated technical results hold for problem **(FSP')**, by modifying Assumption **A** as follows:

Assumption B. **(A1)–(A3)** of Assumption **A** are in effect and:

- (B1)** For a.e. $\omega \in \Omega$ and all $\theta \in \Theta$, the partial (real) Hessian $\frac{\partial^2}{\partial \mathbf{W}^2} F(\mathbf{W}, \mathbf{H}(\theta, \omega)) \Big|_{\mathbf{W}=\mathbf{W}^{\circ}(\theta, \omega)}$ is nonsingular for any $\mathbf{W}^{\circ}(\theta, \omega) \in \{\mathbf{W} \in \mathcal{W} \mid \frac{\partial}{\partial \mathbf{W}} F(\mathbf{W}, \mathbf{H}(\theta, \omega)) = \mathbf{0}\}$;
- (B2)** $F(\mathbf{H}(\mathbf{W}^{\circ}(\theta, \cdot), \cdot), \cdot) \in \mathcal{Z}_2$ is bounded below for any $\theta \in \Theta$ and $\mathbf{W}^{\circ}(\theta, \omega) \in \{\mathbf{W} \in \mathcal{W} \mid \frac{\partial}{\partial \mathbf{W}} F(\mathbf{W}, \mathbf{H}(\theta, \omega)) = \mathbf{0}\}$, and we can draw i.i.d. samples from the law of ω .

An important property of **(FSP')** is that the quality of the critical point given by the oracle (for each (θ, ω)) determines the quality of the approximation of **(FSP)** by **(FSP')**. In practice, one rarely has the ability to choose the “best” out of multiple critical points, but in such a case, choosing the one corresponding to the largest objective value would yield an *optimistic bilevel formulation* (which is equivalent to **(FSP)**, if we can always find a global optimum to the inner problem), while choosing the one corresponding to the smallest objective value would yield a *pessimistic bilevel formulation*. For more information on bilevel programming we refer the reader to [51].

¹The real-derivative can be equivalently substituted by the Wirtinger derivative.

Algorithm ZoSGA Zeroth-order Stochastic Gradient Ascent

Input: $\theta_0 \in \Theta$, $\{\eta_t\}_{t \geq 0} \subset \mathbb{R}_+$, $\mu > 0$, and $T > 0$.
for $(t = 0, 1, 2, \dots, T)$ **do**
 Sample (i.i.d.) $\omega_t \in \Omega$, $\mathbf{U}_t \sim \mathcal{N}(\mathbf{0}, \mathbf{I})$.
 if **(C1)** **then**
 Find $\mathbf{W}^* \in \arg \max_{\mathbf{W} \in \mathcal{W}} F(\mathbf{W}, \mathbf{H}(\theta_t, \omega_t))$.
 else if **(C2)** **then**
 Find $\mathbf{W}^* \in \{\mathbf{W} \in \mathcal{W} \mid \frac{\partial}{\partial \mathbf{W}} F(\mathbf{W}, \mathbf{H}(\theta_t, \omega_t)) = \mathbf{0}\}$.
 end if
 Set $\mathbf{D}_{\mu}(\theta_t, \omega_t, \mathbf{U}_t) \equiv \mathbf{D}_{\mu}(\theta_t, \omega_t, \mathbf{U}_t; \mathbf{W}^*)$ as in (6).
 Update
 $\theta_{t+1} = \text{proj}_{\Theta}(\theta_t + \eta_t \mathbf{D}_{\mu}(\theta_t, \omega_t, \mathbf{U}_t))$.

end for

Sample $t^* \in \{0, \dots, T\}$ according to $\mathbb{P}(t^* = t) = \frac{\eta_t}{\sum_{i=0}^T \eta_i}$.
return θ_{t^*} .

IV. ALGORITHM AND CONVERGENCE ANALYSIS

We are now ready to derive a zeroth-order projected stochastic gradient method for the solution of **(FSP)** or of **(FSP')**. In the former case we assume the availability of an oracle solving the deterministic problem **(SSP)**, while in the latter case we assume the availability of an oracle finding stationary points of **(SSP)**. The method treats the unknown function $\mathbf{H}(\cdot, \omega)$ as a black-box, utilizing samples of the gradient approximation given in (4).

Assumption C. Either of the following is true:

- (C1)** Given any $\theta \in \Theta$ and for a.e. $\omega \in \Omega$, we have access to an oracle yielding a (measurable) optimal solution to **(SSP)**, and Assumption **A** holds.
- (C2)** Given any $\theta \in \Theta$ and for a.e. $\omega \in \Omega$, an oracle yielding some (measurable) stationary point of **(SSP)** is only available, and Assumption **B** holds.

A. A Zeroth-order Projected Stochastic Gradient Ascent

Let us briefly present the proposed (channel-agnostic) zeroth-order projected stochastic gradient ascent. From condition **(A5)** (or, equivalently, **(B2)**), we have available i.i.d. samples $\omega \in \Omega$. Thus, from (5), at every $(\theta, \mathbf{W}) \in \Theta \times \mathcal{W}$, and for a.e. $\omega \in \Omega$, we can utilize the following sample gradient approximation

$$\begin{aligned} & \mathbf{D}_{\mu}(\theta, \omega, \mathbf{U}; \mathbf{W}) \equiv \mathbf{D}_{\mu}(\theta, \omega, \mathbf{U}) \\ & \triangleq \Delta_{\mu}^R \left(\Re \left(\frac{\partial^{\circ}}{\partial \mathbf{z}} F(\mathbf{W}, \mathbf{z}) \Big|_{\mathbf{z}=\mathbf{H}(\theta, \omega)} \right) \right)^{\top} \\ & \quad + \Delta_{\mu}^I \left(\Re \left(j \frac{\partial^{\circ}}{\partial \mathbf{z}} F(\mathbf{W}, \mathbf{z}) \Big|_{\mathbf{z}=\mathbf{H}(\theta, \omega)} \right) \right)^{\top}, \end{aligned} \quad (6)$$

with

$$\begin{aligned} & (\Delta_{\mu}^R, \Delta_{\mu}^I) \\ & \triangleq \frac{1}{\mu} \left[\left(\Re(\Delta_{\mu}(\theta, \omega, \mathbf{U})) \mathbf{U}^{\top} \right)^{\top} \left(\Im(\Delta_{\mu}(\theta, \omega, \mathbf{U})) \mathbf{U}^{\top} \right)^{\top} \right], \end{aligned}$$

where $\mu > 0$ is a smoothing parameter, $\mathbf{U} \sim \mathcal{N}(\mathbf{0}, \mathbf{I})$ and $\Delta_{\mu}(\theta, \omega, \mathbf{U}) \triangleq \mathbf{H}(\theta + \mu \mathbf{U}, \omega) - \mathbf{H}(\theta - \mu \mathbf{U}, \omega)$. Note that this is simply a sample from (5). We are now ready to summarize the proposed method in Algorithm **ZoSGA**.

B. Convergence Analysis

The convergence analysis presented herein covers both (FSP) and (FSP'). In other words, if one has access to an oracle able to find globally optimal solutions to (SSP), the proposed algorithm converges to a local optimum of (FSP), under Assumption A. If, alternatively, one has access to an oracle able to find locally optimal solutions to (SSP), then the proposed algorithm converges to a local optimum of (FSP') under Assumption B.

Let us start by proving certain technical results.

Lemma 6. *Let Assumption C hold, and fix any $\theta \in \Theta$. For a.e. $\omega \in \Omega$ let \mathbf{W} be the output of the oracle at (θ, ω) . Then, for any $\mu \geq 0$, and any $\mathbf{U} \sim \mathcal{N}(\mathbf{0}, \mathbf{I})$, the following holds*

$$\mathbb{E} \left\{ \|\mathbf{D}_\mu(\theta, \omega, \mathbf{U}; \mathbf{W})\|^2 \right\} \leq 4B_F^2 L_{H,0}^2 (S^2 + 2S), \quad (7)$$

where \mathbf{U} and ω are assumed to be statistically independent.

Proof. By Lemma 1, we have that for any $(\theta, \mathbf{W}) \in \Theta \times \mathcal{W}$ and a.e. $\omega \in \Omega$, $\left\| \frac{\partial^\circ}{\partial \mathbf{z}} F(\mathbf{W}, \mathbf{z}) \Big|_{\mathbf{z}=\mathbf{H}(\theta, \omega)} \right\| \leq B_F$. Using the Cauchy-Schwartz inequality, we obtain

$$\begin{aligned} \mathbb{E} \left\{ \|\mathbf{D}_\mu(\theta, \omega, \mathbf{U})\|^2 \right\} &\leq \frac{1}{\mu^2} B_F^2 \mathbb{E} \left\{ \left\| (\Delta_\mu(\theta, \omega, \mathbf{U}) \mathbf{U}^\top)^\top \right\|^2 \right\} \\ &\leq \frac{1}{\mu^2} B_F^2 \mathbb{E} \left\{ \mathbb{E} \left\{ \|\Delta_\mu(\theta, \omega, \mathbf{U})\|^2 \|\mathbf{U}\|^2 \mid \mathbf{U} \right\} \right\} \\ &\leq 4B_F^2 L_{H,0}^2 \mathbb{E} \left\{ \|\mathbf{U}\|^4 \right\} = 4B_F^2 L_{H,0}^2 (S^2 + 2S), \end{aligned}$$

where in the last inequality we used Lipschitz continuity of $\mathbf{H}(\cdot, \omega)$ (from (A3)) while in the last equality we evaluated the 4-th moment of the χ -distribution. By noticing that $F(\mathbf{W}, \mathbf{H}(\theta, \cdot)) \in \mathcal{Z}_2$ from (A5) (or (B2) in the case where (C2) is true), we observe that all of the above expectations are well-defined and finite and hence the proof is complete. \square

Lemma 7. *Let Assumption C hold, fix any $\theta \in \Theta$, and for a.e. $\omega \in \Omega$, let \mathbf{W} be the output of the oracle. Then, the sample gradient approximation given in (6) satisfies*

$$\begin{aligned} \mathbb{E} \left\{ \mathbf{D}_\mu(\theta, \omega, \mathbf{U}; \mathbf{W}) \right\} &= \mathbb{E} \left\{ \nabla_\theta^\mu F(\mathbf{W}, \mathbf{H}(\theta, \omega)) \right\} \triangleq \widehat{\nabla} f(\theta), \\ \left\| \widehat{\nabla} f(\theta) - \nabla f(\theta) \right\| &\leq 2\mu B_F L_{H,1} \sqrt{MS}. \end{aligned}$$

Proof. Firstly, by utilizing Fubini's theorem we obtain that

$$\mathbb{E} \left\{ \mathbf{D}_\mu(\theta, \omega, \mathbf{U}; \mathbf{W}) \right\} = \mathbb{E} \left\{ \nabla_x^\mu F(\mathbf{W}, \mathbf{H}(\theta, \omega)) \right\},$$

where the first expectation is taken with respect to the product measure of the two random variables ω and \mathbf{U} . Furthermore,

$$\begin{aligned} &\left\| \nabla_\theta^\mu F(\mathbf{W}, \mathbf{H}(\theta, \omega)) - \nabla_\theta F(\mathbf{W}, \mathbf{H}(\theta, \omega)) \right\| \\ &= \left\| 2\Re \left(\frac{\partial^\circ}{\partial \mathbf{z}} F(\mathbf{W}, \mathbf{z}) \Big|_{\mathbf{z}=\mathbf{H}(\theta, \omega)} (\varepsilon^R + j\varepsilon^I) \right) \right\| \\ &\leq 2B_F \|\varepsilon^R + j\varepsilon^I\| \end{aligned}$$

where $\varepsilon^R \triangleq \nabla_\theta \Re(\mathbf{H}(\theta, \omega)) - \nabla_\theta \mathbf{H}_\mu^R(\theta, \omega)$ and $\varepsilon^I \triangleq \nabla_\theta \Im(\mathbf{H}(\theta, \omega)) - \nabla_\theta \mathbf{H}_\mu^I(\theta, \omega)$, and we used Lemma 1. Next, we observe (from equivalence of norms) that

$$\begin{aligned} \|\varepsilon^R\| &\leq \sqrt{M} \max_i \left\| (\nabla_\theta \Re(\mathbf{H}(\theta, \omega)) - \nabla_\theta \mathbf{H}_\mu^R(\theta, \omega))_i \right\| \\ &\leq \frac{\mu}{2} L_{H,1} \sqrt{MS}, \end{aligned}$$

where, given a matrix \mathbf{A} , $(\mathbf{A})_i$ denotes the i -th column vector, and the last bound follows as in the proof of [60, Theorem 1]. The same procedure can be repeated for bounding $\|j\varepsilon^I\|$ and hence a simple application of the triangle inequality and subsequently Jensen's inequality yield the desired result. \square

The Moreau envelope: Let us write the objective function of (FSP) (or (FSP')), respectively) as $\phi(\theta) \triangleq -f(\theta) + \delta_\Theta(\theta)$, where $\delta_\Theta(\theta)$ is the indicator function for the convex set Θ . Given some penalty parameter $\lambda > 0$, we define the proximity operator as

$$\mathbf{prox}_{\lambda\phi}(\mathbf{u}) \triangleq \arg \min_{\theta \in \mathbb{R}^S} \left\{ \phi(\theta) + \frac{1}{2\lambda} \|\mathbf{u} - \theta\|^2 \right\},$$

and the corresponding Moreau envelope as

$$\phi^\lambda(\mathbf{u}) \triangleq \min_{\theta \in \mathbb{R}^S} \left\{ \phi(\theta) + \frac{1}{2\lambda} \|\mathbf{u} - \theta\|^2 \right\}.$$

It is well-known that the Moreau envelope with parameter $\lambda > \rho$ (the weak convexity constant) is smooth even if $\phi(\cdot)$ is not, and the magnitude of its gradient can be used as a near-stationarity measure of the non-smooth problem of interest. This approach is adopted in this work, following [55], [59], among others.

Theorem 8. *Let Assumption C be in effect and assume that $\{\theta_t\}_{t=0}^T$, $T > 0$, is a sequence of iterates generated by Algorithm ZoSGA, where θ_{t^*} is the point that the algorithm returns. For any $\bar{\rho} > \rho$, it holds that*

$$\begin{aligned} &\mathbb{E} \left\{ \left\| \nabla \phi^{1/\bar{\rho}}(\theta_{t^*}) \right\|^2 \right\} \\ &\leq \frac{\bar{\rho}}{\bar{\rho} - \rho} \left(\frac{\phi^{1/\bar{\rho}}(x_0) - \min \phi(x) + C_2 \bar{\rho} \sum_{t=0}^T \eta_t^2}{\sum_{t=0}^T \eta_t} + C_1 \bar{\rho} \mu \right) \end{aligned} \quad (8)$$

where, letting Δ_Θ be the diameter of Θ ,

$$C_1 \triangleq 2\Delta_\Theta B_F L_{H,1} \sqrt{MS}, \quad C_2 \triangleq 2B_F^2 L_{H,0}^2 (S^2 + 2S).$$

Moreover, if we set $\bar{\rho} = 2\rho$, and

$$\eta_t = \sqrt{\frac{\Delta_f}{2C_2 \rho (T+1)}}, \quad \text{for all } t \geq 0,$$

for some $\Delta_f \geq \phi^{1/(2\rho)}(\theta_0) - \min \phi(\theta)$, then it holds that

$$\mathbb{E} \left\{ \left\| \nabla \phi^{1/(2\rho)}(\theta_{t^*}) \right\|^2 \right\} \leq 8 \left(\sqrt{\frac{\Delta_f \rho C_2}{2(T+1)}} + C_1 \rho \mu \right). \quad (9)$$

Proof. For any $t \geq 0$, we have $\widehat{\nabla} f(\theta_t) \equiv \mathbb{E}_{[t]} \left\{ \mathbf{D}_\mu(\theta, \omega, \mathbf{U}) \right\}$, where $\mathbb{E}_{[t]} \{ \cdot \} \triangleq \mathbb{E} \{ \cdot \mid \mathbf{U}_{t-1}, \omega_{t-1}, \dots, \mathbf{U}_0, \omega_0 \}$ (see Lemma 7).

We define the point $\hat{\boldsymbol{\theta}}_t \triangleq \mathbf{prox}_{\phi/\bar{\rho}}(\boldsymbol{\theta}_t)$. Then, we obtain

$$\begin{aligned}
\mathbb{E}_{[t]} \left\{ \phi^{1/\bar{\rho}}(\boldsymbol{\theta}_{t+1}) \right\} &\leq \mathbb{E}_{[t]} \left\{ f(\hat{\boldsymbol{\theta}}_t) + \frac{\bar{\rho}}{2} \|\hat{\boldsymbol{\theta}}_t - \boldsymbol{\theta}_{t+1}\|^2 \right\} \\
&= \phi(\hat{\boldsymbol{\theta}}_t) + \frac{\bar{\rho}}{2} \mathbb{E}_{[t]} \left\{ \|\mathbf{proj}_{\Theta}(\hat{\boldsymbol{\theta}}_t) \right. \\
&\quad \left. - \mathbf{proj}_{\Theta}(\boldsymbol{\theta}_t + \eta_t \mathbf{D}_{\mu}(\boldsymbol{\theta}_t, \omega_t, \mathbf{U}_t))\|^2 \right\} \\
&\leq \phi(\hat{\boldsymbol{\theta}}_t) + \frac{\bar{\rho}}{2} \mathbb{E}_{[t]} \left\{ \|\boldsymbol{\theta}_t + \eta_t \mathbf{D}_{\mu}(\boldsymbol{\theta}_t, \omega_t, \mathbf{U}_t) - \hat{\boldsymbol{\theta}}_t\|^2 \right\} \\
&\leq \phi(\hat{\boldsymbol{\theta}}_t) + \frac{\bar{\rho}}{2} \|\boldsymbol{\theta}_t - \hat{\boldsymbol{\theta}}_t\|^2 \\
&\quad + \bar{\rho} \eta_t \mathbb{E}_{[t]} \left\{ \left\langle \hat{\boldsymbol{\theta}}_t - \boldsymbol{\theta}_t, -\mathbf{D}_{\mu}(\boldsymbol{\theta}_t, \omega_t, \mathbf{U}_t) \right\rangle \right\} + C_2 \bar{\rho} \eta_t^2 \\
&= \phi(\hat{\boldsymbol{\theta}}_t) + \frac{\bar{\rho}}{2} \|\boldsymbol{\theta}_t - \hat{\boldsymbol{\theta}}_t\|^2 + \bar{\rho} \eta_t \left\langle \hat{\boldsymbol{\theta}}_t - \boldsymbol{\theta}_t, -\nabla f(\boldsymbol{\theta}) \right\rangle \\
&\quad + \bar{\rho} \eta_t \left\langle \hat{\boldsymbol{\theta}}_t - \boldsymbol{\theta}_t, \nabla f(\boldsymbol{\theta}_t) - \hat{\nabla} f(\boldsymbol{\theta}_t) \right\rangle + C_2 \bar{\rho} \eta_t^2 \\
&\leq \phi^{1/\bar{\rho}}(\boldsymbol{\theta}_t) + \bar{\rho} \eta_t \left\langle \hat{\boldsymbol{\theta}}_t - \boldsymbol{\theta}_t, -\nabla f(\boldsymbol{\theta}) \right\rangle \\
&\quad + \bar{\rho} \eta_t \left\| \hat{\boldsymbol{\theta}}_t - \boldsymbol{\theta}_t \right\| \left\| \hat{\nabla} f(\boldsymbol{\theta}) - \nabla f(\boldsymbol{\theta}) \right\| + C_2 \bar{\rho} \eta_t^2 \\
&\leq \phi^{1/\bar{\rho}}(\boldsymbol{\theta}_t) + \bar{\rho} \eta_t \left(f(\boldsymbol{\theta}_t) - f(\hat{\boldsymbol{\theta}}_t) + \frac{\rho}{2} \|\boldsymbol{\theta}_t - \hat{\boldsymbol{\theta}}_t\|^2 \right) \\
&\quad + C_1 \bar{\rho} \mu \eta_t + C_2 \bar{\rho} \eta_t^2,
\end{aligned}$$

where in the second inequality we used the non-expansiveness of the projection operator, in the fourth inequality we used Cauchy-Schwartz as well as the definition of the Moreau envelope, and in the fifth inequality we have used the weak convexity of $-f(\cdot)$, as well as Lemma 7 and the fact that Θ is assumed to be compact and hence there exists a constant $\Delta_{\Theta} > 0$ such that $\|\hat{\boldsymbol{\theta}}_t - \boldsymbol{\theta}_t\| \leq \Delta_{\Theta}$. Next, by following exactly the developments in [55, Section 3.1], we notice that the mapping $\boldsymbol{\theta} \mapsto -f(\boldsymbol{\theta}) + \frac{\rho}{2} \|\boldsymbol{\theta} - \boldsymbol{\theta}_t\|^2$ is strongly convex with parameter $\bar{\rho} - \rho$, and hence

$$f(\hat{\boldsymbol{\theta}}_t) - f(\boldsymbol{\theta}_t) \geq (\bar{\rho} - \rho) \|\boldsymbol{\theta}_t - \hat{\boldsymbol{\theta}}_t\|^2 \equiv \frac{\bar{\rho} - \rho}{\bar{\rho}^2} \|\nabla \phi^{1/\bar{\rho}}(\boldsymbol{\theta}_t)\|^2,$$

where the last equivalence follows from [55, Lemma 2.2]. Hence,

$$\begin{aligned}
\mathbb{E}_{[t]} \left\{ \phi^{1/\bar{\rho}}(\boldsymbol{\theta}_{t+1}) \right\} &\leq \phi^{1/\bar{\rho}}(\boldsymbol{\theta}_t) - \frac{\eta_t(\bar{\rho} - \rho)}{\bar{\rho}} \|\nabla \phi^{1/\bar{\rho}}(\boldsymbol{\theta}_t)\|^2 \\
&\quad + C_1 \bar{\rho} \mu \eta_t + C_2 \bar{\rho} \eta_t^2.
\end{aligned}$$

Taking expectations with respect to the history $\omega_0, \mathbf{U}_0, \dots, \omega_{t-1}, \mathbf{U}_{t-1}$ and using the total expectation, yields

$$\begin{aligned}
\mathbb{E} \left\{ \phi^{1/\bar{\rho}}(\boldsymbol{\theta}_{t+1}) \right\} &\leq \mathbb{E} \left\{ \phi^{1/\bar{\rho}}(\boldsymbol{\theta}_t) \right\} + \bar{\rho} \eta_t (\mu C_1 + C_2 \eta_t) \\
&\quad - \frac{\eta_t(\bar{\rho} - \rho)}{\bar{\rho}} \mathbb{E} \left\{ \|\nabla \phi^{1/\bar{\rho}}(\boldsymbol{\theta}_t)\|^2 \right\},
\end{aligned}$$

Subsequently, we can unfold the latter inequality to obtain

$$\begin{aligned}
\mathbb{E} \left\{ \phi^{1/\bar{\rho}}(\boldsymbol{\theta}_{T+1}) \right\} &\leq \phi^{1/\bar{\rho}}(\boldsymbol{\theta}_0) + C_1 \bar{\rho} \mu \sum_{t=0}^T \eta_t + C_2 \bar{\rho} \sum_{t=0}^T \eta_t^2 \\
&\quad - \frac{\bar{\rho} - \rho}{\bar{\rho}} \sum_{t=0}^T \eta_t \mathbb{E} \left\{ \|\nabla \phi^{1/\bar{\rho}}(\boldsymbol{\theta}_t)\|^2 \right\}.
\end{aligned}$$

Then, we can lower bound the left-hand side by $\phi(\boldsymbol{\theta}^*) \triangleq \min_{\boldsymbol{\theta} \in \Theta} f(\boldsymbol{\theta})$, and rearrange, to obtain

$$\begin{aligned}
&\frac{1}{\sum_{t=0}^T \eta_t} \sum_{t=0}^T \eta_t \mathbb{E} \left\{ \|\nabla \phi^{1/\bar{\rho}}(\boldsymbol{\theta}_t)\|^2 \right\} \\
&\leq \frac{\bar{\rho}}{\bar{\rho} - \rho} \left(\frac{\phi^{1/\bar{\rho}}(\boldsymbol{\theta}_0) - \phi(\boldsymbol{\theta}^*) + C_2 \bar{\rho} \sum_{t=0}^T \eta_t^2}{\sum_{t=0}^T \eta_t} + C_1 \bar{\rho} \mu \right).
\end{aligned}$$

Since the left-hand side is exactly $\mathbb{E}\{\|\nabla \phi^{1/\bar{\rho}}(\boldsymbol{\theta}_{t^*})\|^2\}$, we deduce that (8) holds. Finally, setting $\bar{\rho} = 2\rho$, letting $\Delta_f \geq \phi^{1/\bar{\rho}}(\boldsymbol{\theta}_0) - \min \phi(\boldsymbol{\theta})$, and choosing a constant step size as

$$\eta_t = \sqrt{\frac{\Delta_f}{2C_2(T+1)}}, \quad \text{for all } t \geq 0,$$

we obtain (9) which completes the proof. \square

Remark 3. Note that choosing $\mu = \mathcal{O}(1/\sqrt{MT})$ yields that $\mathbb{E}\{\|\nabla \varphi^{1/(2\rho)}(\boldsymbol{\theta}_{t^*})\|\} \leq \epsilon$, after $\mathcal{O}(\sqrt{S}\epsilon^{-4})$ iterations.

V. CASE STUDY: SUMRATE MAXIMIZATION

Capitalizing on a standard IRS-aided MISO downlink scenario (also see Figure 2 in Section VI), our goal here is to maximize the total downlink rate of K users actively serviced by an AP with M antennas, while passively aided by one or multiple IRSs, arbitrarily spatially placed. As usual, we assume dynamic (reactive) AP precoders, while the IRS beamformers are static (non-reactive) tunable elements. We make no sensing assumptions on the IRSs, i.e., the IRSs are completely passive network elements.

Each user $k = 1, \dots, K$ experiences a random effective channel denoted by $\mathbf{h}_k(\boldsymbol{\theta}, \omega)$, indexed by the IRS parameter vector $\boldsymbol{\theta}$ as well as the usual state of nature $\omega \in \Omega$ describing *unobservable* random propagation patterns for each value of $\boldsymbol{\theta}$. In other words, $\mathbf{h}_k(\boldsymbol{\theta}, \omega)$ is a random channel field with spatial variable $\boldsymbol{\theta}$. We make the standard assumption that the effective channels $\mathbf{h}_k(\boldsymbol{\theta}, \omega), k = 1, \dots, K$, are known to the AP at the time of transmission [20], [21]. Note that the implementation complexity of estimating effective channels in our setting is exactly the same as that in conventional multi-user downlink beamforming (i.e., involving no IRSs), *regardless* of the number and/or spatial configuration of the IRSs; no extra hardware or customized scheduling schemes (such as those in [21]) are required on either the AP or the IRSs assisting the network.

The QoS of user k is measured by the corresponding SINR,

$$\text{SINR}_k(\mathbf{W}, \mathbf{h}_k(\boldsymbol{\theta}, \omega)) \triangleq \frac{|\mathbf{h}_k^H(\boldsymbol{\theta}, \omega) \mathbf{w}_k|^2}{\sum_{j \in \mathbb{N}_K^+ \setminus k} |\mathbf{h}_k^H(\boldsymbol{\theta}, \omega) \mathbf{w}_j|^2 + \sigma_k^2},$$

where $\mathbf{W} = [\mathbf{w}_1 \ \mathbf{w}_2 \ \dots \ \mathbf{w}_K] \in \mathbb{C}^{M \times K}$, \mathbf{w}_k is a transmit precoding vector and σ_k^2 is the noise variance for user k , respectively. Then, the *weighted sumrate utility* of the network is defined as

$$F(\mathbf{W}, \mathbf{H}(\boldsymbol{\theta}, \omega)) \triangleq \sum_{k=1}^K \alpha_k \log_2(1 + \text{SINR}_k(\mathbf{W}, \mathbf{h}_k(\boldsymbol{\theta}, \omega))),$$

with $\mathbf{H} = [\mathbf{h}_1 \ \dots \ \mathbf{h}_K] \in \mathbb{C}^{M \times K}$, and $\alpha_k \geq 0$ the weight associated with user k . We are interested in maximizing the sumrate of the network jointly by selecting instantaneous-optimal

dynamic AP precoders \mathbf{W} , and on-average-optimal static IRS beamformers $\boldsymbol{\theta}$ [20], [21], i.e., we are interested in the problem

$$\max_{\boldsymbol{\theta} \in \Theta} \mathbb{E} \left\{ \max_{\mathbf{W}: \|\mathbf{W}\|_F^2 \leq P} F(\mathbf{W}, \mathbf{H}(\boldsymbol{\theta}, \omega)) \right\}, \quad (10)$$

where $\|\cdot\|_F^2$ denotes the Frobenius norm, $P > 0$ is a total power budget at the AP, and Θ is a convex and compact feasible set. Problem (10) is an instance of (2SP). Following the discussion in Section III-E, we also define an approximation of (10), as:

$$\max_{\boldsymbol{\theta} \in \Theta} \mathbb{E} \{ F(\mathbf{W}^\diamond(\boldsymbol{\theta}, \omega), \mathbf{H}(\boldsymbol{\theta}, \omega)) \}, \quad (11)$$

where

$$\mathbf{W}^\diamond(\boldsymbol{\theta}, \omega) \in \left\{ \mathbf{W} \in \mathbb{C}^{D \times K} \mid \|\mathbf{W}\|_F^2 \leq P, \right. \\ \left. \frac{\partial}{\partial \mathbf{W}} F(\mathbf{W}, \mathbf{H}(\boldsymbol{\theta}, \omega)) = \mathbf{0} \right\}.$$

Assumption Compatibility: In what follows, we briefly discuss the compatibility of Assumption A (resp. Assumption B) with problem (10) (resp. problem (11)). To that end, we firstly note that conditions (A1), (A2) are both satisfied. Condition (A5) (resp. (B2)) is also satisfied in light of uniform boundedness. Let us now showcase that the regularity condition (A4) (resp. (B1)) can also hold, with probability 1, given (A3). To see this, note that given some arbitrary bounded random variable δ such that $\mathbb{E}\{\delta\} = 0$, we can alternatively solve the regularized version of (2SP)

$$\max_{\boldsymbol{\theta} \in \Theta} \mathbb{E} \left\{ \max_{\mathbf{W}: \|\mathbf{W}\|_F^2 \leq P} \left\{ F(\mathbf{W}, \mathbf{H}(\boldsymbol{\theta}, \omega)) + \frac{\delta}{2} \mathbf{W}^H \mathbf{W} \right\} \right\},$$

assuming that δ is independent of $\mathbf{H}(\cdot, \omega)$. Our assumption that $\mathbb{E}\{\delta\} = 0$ implies that the objective value of the problem under study does not change. We observe that, with probability 1, the partial Hessian of the inner objective function is nonsingular, and hence (A4) (resp. (B1)) is justified.

In other words, when considering problem (10) (resp. problem (11)), our theory requires only condition (A3) of Assumption A. This condition imposes regularity that is required for the grounded development of our optimization scheme and for its convergence analysis. Also, observe that the boundedness assumption is natural, since (IRS-aided) wireless channels are always bounded in practice. While we usually have no information on the analytical properties of the effective channel, this condition is easily satisfied in widely used channel models of IRS-aided systems, see, e.g., [21] as well as Section VI.

VI. SIMULATIONS

Building upon the IRS-aided MISO downlink sumrate maximization case discussed in Section V, we present a set of detailed simulations to empirically evaluate and confirm the efficacy of the proposed ZoSGA algorithm. Unless stated otherwise, all our empirical results are averaged over 2000 independent simulations, with an additional 4-th order Savitzky–Golay filter [61] of length 500, while 95% confidence intervals are also provided. In what follows, we describe and evaluate three distinct wireless network setups and examine the obtained empirical results. The last set of experiments will involve a physical model for the IRSs, which is briefly described in the beginning of Subsection VI-C.

A. Baseline Channel Model

With the practically feasible assumption of insufficient angular spread of signals in a scattering environment, we consider both LOS and non-LOS channels. Following [21], we consider three types of intermediate channels in the presented simulations, namely, the direct path channel $\mathbf{h}_{d,k}$ from an AP to user k , the channel \mathbf{G} from an AP to an IRS, and the reflected channel $\mathbf{h}_{r,k}$ from an IRS to user k . We model these as general spatially correlated Rician fading channels [62]. Additionally, we assume that the second-order statistics of the LOS links are identical for all users, due to the large distances between an AP and its served users. Concretely, for each user k , we define these channels as

$$\mathbf{h}_{r,k} \triangleq \sqrt{\frac{\beta_{Iu}}{1+\beta_{Iu}}} \check{\mathbf{v}}_{r,k} + \sqrt{\frac{1}{1+\beta_{Iu}}} \boldsymbol{\Phi}_{r,k}^{1/2} \mathbf{v}_{r,k}, \\ \mathbf{G} \triangleq \sqrt{\frac{\beta_{AI}}{1+\beta_{AI}}} \check{\mathbf{F}} + \sqrt{\frac{1}{1+\beta_{AI}}} \boldsymbol{\Phi}_r^{1/2} \mathbf{F} \boldsymbol{\Phi}_d^{1/2}, \quad (12) \\ \mathbf{h}_{d,k} \triangleq \sqrt{\frac{\beta_{Au}}{1+\beta_{Au}}} \check{\mathbf{v}}_{d,k} + \sqrt{\frac{1}{1+\beta_{Au}}} \boldsymbol{\Phi}_d^{1/2} \mathbf{v}_{d,k},$$

where $\mathbf{v}_{r,k} \in \mathbb{C}^{N \times 1}$, $\mathbf{F} \in \mathbb{C}^{N \times M}$, and $\mathbf{v}_{d,k} \in \mathbb{C}^{M \times 1}$ are the instantaneous components (I-CSI), and $\check{\mathbf{v}}_{r,k} \in \mathbb{C}^{N \times 1}$, $\check{\mathbf{F}} \in \mathbb{C}^{N \times M}$, and $\check{\mathbf{v}}_{d,k} \in \mathbb{C}^{M \times 1}$ are the statistical components (S-CSI) of the above channels, all having i.i.d. circularly symmetric complex Gaussian (CSCG) entries with zero mean and unit variance, and with S-CSI being sampled once per simulation. The dimensions M and N denote the number of AP antennas and the number of passive reflective elements in an IRS, respectively. The matrices $\boldsymbol{\Phi}_{r,k} \in \mathbb{C}^{N \times N}$, $\boldsymbol{\Phi}_d \in \mathbb{C}^{M \times M}$, and $\boldsymbol{\Phi}_r \in \mathbb{C}^{N \times N}$ are, in order, the reflected channel correlation matrix, the AP transmit correlation matrix, and the IRS receive correlation matrix. We assume an exponential correlation model for $\boldsymbol{\Phi}_d$ [63], expressed as

$$\boldsymbol{\Phi}_d(i, j) = \begin{cases} r_d^{j-i}, & \text{if } i \leq j, \\ \boldsymbol{\Phi}_d(j, i), & \text{if } i > j, \end{cases} \quad (13)$$

where $r_d \in (0, 1)$ is the correlation coefficient. The matrices $\boldsymbol{\Phi}_r$ and $\boldsymbol{\Phi}_{r,k}$ are modeled as Kronecker products [64] as

$$\boldsymbol{\Phi}_r = \boldsymbol{\Phi}_r^h \otimes \boldsymbol{\Phi}_r^v, \quad \boldsymbol{\Phi}_{r,k} = \boldsymbol{\Phi}_{r,k}^h \otimes \boldsymbol{\Phi}_{r,k}^v,$$

where $\boldsymbol{\Phi}_r^h$, $\boldsymbol{\Phi}_{r,k}^h$, and $\boldsymbol{\Phi}_r^v$, $\boldsymbol{\Phi}_{r,k}^v$, for $k \in \mathbb{N}_K^+$, represent the spatial correlation matrices of the horizontal and vertical domains, respectively, and are all modeled similar to $\boldsymbol{\Phi}_d$ in (13), with spatial correlation coefficients $r_r \in (0, 1)$ and $r_{r,k} \in (0, 1)$ for $\boldsymbol{\Phi}_r$, and $\boldsymbol{\Phi}_{r,k}$, $k \in \mathbb{N}_K^+$, respectively.

The deterministic components, i.e., $\check{\mathbf{v}}_{r,k}$, $\check{\mathbf{F}}$, and $\check{\mathbf{v}}_{d,k}$ determine the moments of their respective CSIs. Lastly, the real scalar β_{Au} denotes the Rician fading factor for the LOS channel, while β_{Iu} and β_{AI} are the same for the reflected channels. These factors define the relative dominance of I-CSIs and S-CSIs in their respective combined CSIs. Moreover, all intermediate channels in (12) suffer from an exponential path loss proportional to the path distance. We model this loss as $L_{path} = \sqrt{C_0 d_{path}^{-\alpha}}$, where d_{path} is the path distance in meters, α is the path loss exponent depending upon the channel being considered, and C_0 is the path-loss for when the path distance is one meter.

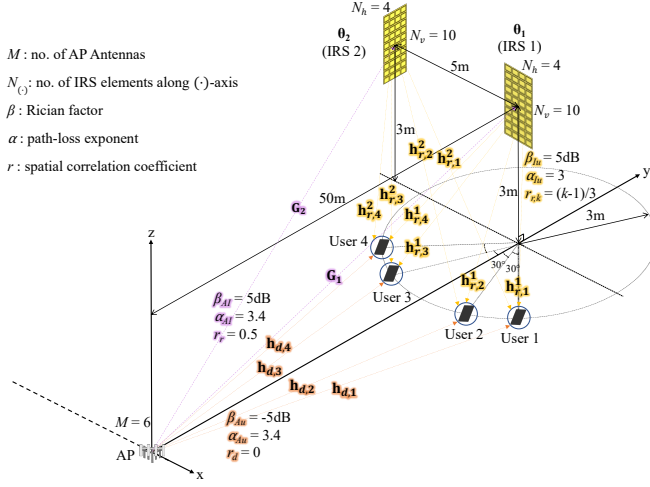


Fig. 2: First IRS-aided network configuration (ideal IRSs).

Considering the above, we may adopt the standard simplified baseline model for the effective channel $\mathbf{h}_k(\boldsymbol{\theta}, \omega)$ of user k in the presence of an AP and *one* IRS as

$$\mathbf{h}_k(\boldsymbol{\theta}, \omega) \triangleq \underbrace{\mathbf{G}^H \text{Diag}(\mathbf{A} \circ e^{j\phi}) \mathbf{h}_{r,k}}_{\text{non-LOS link}} + \underbrace{\mathbf{h}_{d,k}}_{\text{LOS link}},$$

where we may take $\omega = \{\mathbf{G}, \mathbf{h}_{r,k}, \mathbf{h}_{d,k}, k \in \mathbb{N}_K^+\}$ and the IRS parameters $\boldsymbol{\theta}$ are represented by amplitude and phase vectors $\mathbf{A} \in [0, 1]^N$ and $\phi \in [-2\pi, 2\pi]^N$, respectively [65]. Adding more IRSs to the system increases the non-LOS terms comprising the effective channel of each user accordingly.

For slow moving users, as is generally the case, we assume that the values of S-CSI and the spatial correlation matrices remain fixed throughout the duration of the AP service. Further, we assume that IRS-to-IRS links do not contribute to the signal or the interference in the presented multi-IRS cases. Of course, the latter assumption is only made for ease of presentation.

In Subsections VI-B and VI-C, having defined the channel model, we present simulated results with ideal and physical IRSs, where physical IRSs are constrained both in terms of amplitude and phase, as well as non-linear sensitivity relative to the action space, i.e., the ranges of varactor diode capacitances [66].

B. Networks with Ideal IRSs

In the first set of our simulations, we assume that we have full control over the amplitudes and the phases of an IRS phase-shift elements, i.e. there is no constraint on achievable phase-amplitude pairs, and we can control these directly. We start by discussing the wireless network setting as shown in Figure 2.

To highlight the efficacy of the presence of IRSs in a wireless network, we assume a more acute signal attenuation in the LOS path from the AP to the users. Thus, we set $\alpha_{Au} = 3.4$, $\alpha_{Iu} = 3$ and $\alpha_{AI} = 2.2$, where the largest α_{Au} is the LOS path loss exponent while the remaining two are path loss exponents of IRS-User and AP-IRS links, respectively. Moreover, since the distances between the IRS and its served users are relatively small, IRS elements reflect signals with a finite angular spread and a user-location dependent mean angle in practice [67].

We consider two IRSs, as shown in Figure 2, equipped with $N = N_h \times N_v$ rectangular phase-shift elements where $N_h (= 4)$

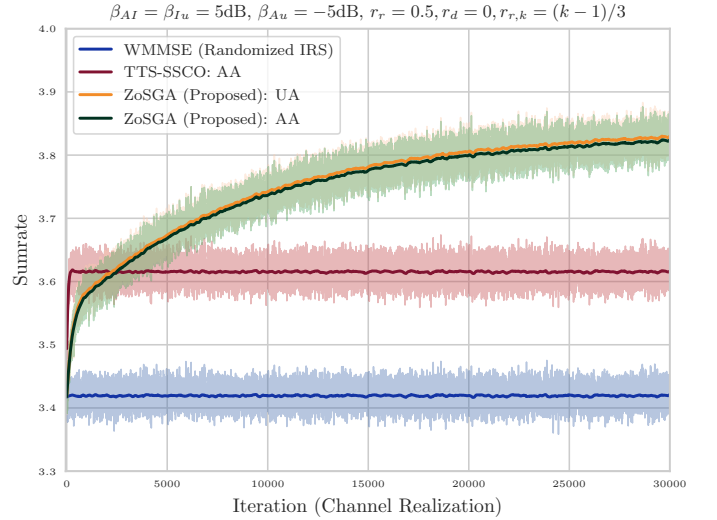


Fig. 3: Average system sumrates achieved by WMMSE [50] (random IRS phase-shifts), TTS-SSCO [21], and ZoSGA, with only IRS 1 present (AA: Adjustable Amplitude; UA: Unit Amplitude).

and $N_v (= 10)$ denote the number of columns and rows, respectively ($N = 40$). For the ideal case we define the controllable parameters of each IRS as a vector $\boldsymbol{\theta}_i = [\boldsymbol{\phi}_i^T \mathbf{A}_i^T]^T$, for $i \in \{1, 2\}$, where $\boldsymbol{\phi}_i \in [-2\pi, 2\pi]^N$ and $\mathbf{A}_i \in [0, 1]^N$ are phases and amplitudes of the IRS elements, respectively. We do not consider the relative orientations of IRSs, AP and users, as those can be incorporated via rotation offsets, if needed. The effective channel for a user k can, thus, be expressed as

$$\mathbf{h}_k(\boldsymbol{\theta}, \omega) = \sum_{i=1}^2 \underbrace{\mathbf{G}_i^H \text{Diag}(\mathbf{A}_i \circ e^{j\phi_i}) \mathbf{h}_{r,k}^i}_{\boldsymbol{\theta}_i\text{-non-LoS link}} + \underbrace{\mathbf{h}_{d,k}}_{\text{LoS link}},$$

where $\boldsymbol{\theta} = (\boldsymbol{\theta}_1, \boldsymbol{\theta}_2)$ and $\omega = \{\mathbf{G}_1, \mathbf{G}_2, \mathbf{h}_{r,k}^1, \mathbf{h}_{r,k}^2, \mathbf{h}_{d,k}, k \in \mathbb{N}_K^+\}$.

After defining the wireless network setting, we move forward with our simulations. In the first simulated comparison we compare the proposed algorithm (ZoSGA) with the well-documented Stochastic Successive Convex Optimization (SSCO) method, specifically a version of it proposed in [21], which we shall refer to as Two-Time Scale SSCO (TTS-SSCO). Both ZoSGA and TTS-SSCO employ the WMMSE algorithm to optimize the precoding vectors. To keep the comparison justified, we let WMMSE optimize for 20 iterations per channel instance for both of these methods, and have also included WMMSE with randomized IRS parameters as a reference. All parameters pertaining to the TTS-SSCO are taken from [21, Section V], i.e., $T_H = 10$, $\tau = 0.01$, $\rho_t = t^{-0.8}$ and $\gamma_t = t^{-1}$. There are four users, so $k \in \mathbb{N}_4^+$, weighted uniformly i.e., $\alpha_k = 1$; the AP has six antennas ($M = 6$), and the noise variance is $\sigma_k = -80\text{dBm}$ for all k . The reference path loss is $C_0 = -30\text{dB}$, and the total allocated power budget is $P = 5\text{dBm}$. The LOS Rician factor is $\beta_{Au} = -5\text{dB}$, while $\beta_{Iu} = \beta_{AI} = 5\text{dB}$, unless specified otherwise. We let the smoothing parameter $\mu = 10^{-12}$ in Algorithm ZoSGA, and choose separate initial step-sizes $\eta_\phi^0 = 0.4$ and $\eta_A^0 = 0.01$ for updating phases and amplitudes, respectively, scaled by 0.9972^t for $t \in \mathbb{N}_{10^3}^+$, keeping them constant for $t > 10^3$.

The comparison of ZoSGA and TTS-SSCO in terms of achieved sumrate is shown in Figure 3. The comparison is done

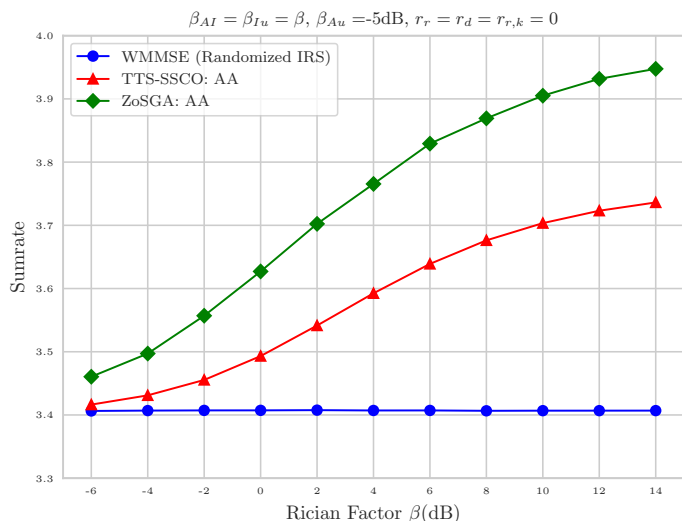


Fig. 4: Average system sumrates versus the Rician factor achieved by WMMSE [50] (with random IRS phase-shifts), TTS-SSCO [21], and ZoSGA, with only IRS 1 present.

with only IRS 1 present, matching the TTS-SSCO setting in [21], which requires exact channel and network models to work. We observe that ZoSGA substantially outperforms TTS-SSCO solely on the basis of effective CSI, while having no access to the statistical model of the channel or the spatial configuration of the system. There are two main reasons for this. Firstly, TTS-SSCO evaluates gradients by utilizing internally sampled I-CSI and the corresponding optimal precoding vectors (via WMMSE), with a frequency of ten samples per iteration (T_H). This can greatly limit the convergence of TTS-SSCO if the internal channel model is not accurate. Secondly, the surrogate objective employed by TTS-SSCO is not equivalent to the original sumrate optimization problem. As shown by the convergence curves provided in Figure 3, this introduces additional errors, preventing TTS-SSCO from realizing a competitive QoS gain, compared with ZoSGA.

In Figure 4, we discern the effect of the Rician factor for spatially uncorrelated channels, i.e., we set $r_d = r_r = r_{r,k} = 0$, $\forall k \in \mathbb{N}_4^+$. We observe that the relative gain of ZoSGA in the achievable sumrate increases with respect to the Rician factors pertaining to θ_1 -reflected links, i.e., as we move from I-CSI to S-CSI dominated channels. The gain difference between ZoSGA and TTS-SSCO increases in β , since in a close-to-deterministic effective channel zeroth-order gradient approximations approach the true gradients, while TTS-SSCO is optimizing an approximate surrogate objective. We also observe that WMMSE with a randomized IRS remains insensitive to changes in the Rician factors; this is expected as the reflected channel is not optimized to gain any performance improvements.

We can now verify that ZoSGA can indeed optimize networks with multiple IRSs without any model knowledge. We do so by tuning both IRSs as shown in Figure 2, while keeping the same hyper-parameters for ZoSGA as well as for WMMSE. Figure 5 shows that ZoSGA succeeds in optimizing both IRSs simultaneously, without any information about their spatial configuration. Figure 5 also demonstrates the improved performance gains when optimizing θ_1 versus optimizing the more distant θ_2 , showing that ZoSGA not only scales well to unknown system/channel

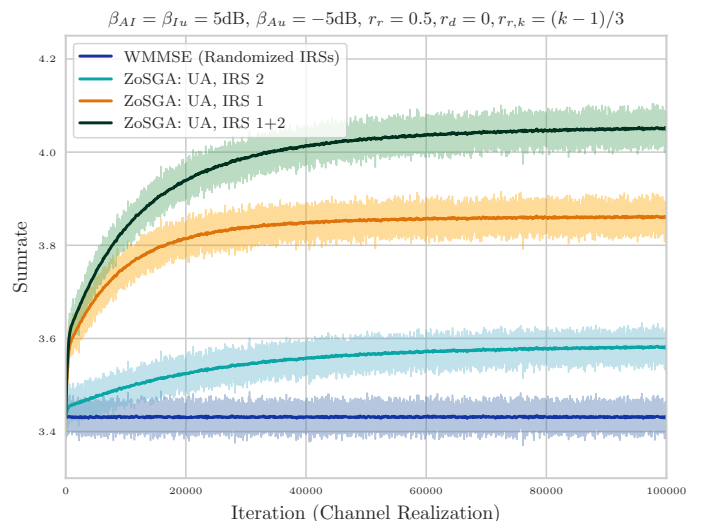


Fig. 5: Average system sumrates achieved by WMMSE [50] (with random IRS phase-shifts) and ZoSGA, with both IRSs present.

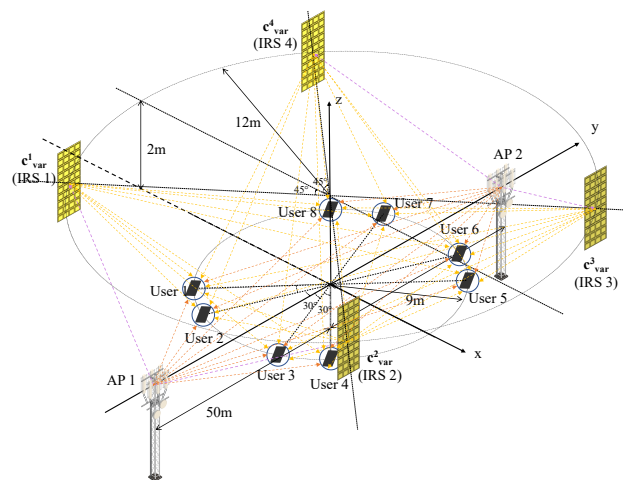


Fig. 6: Second IRS-aided network configuration (physical IRSs) models, but is also robust with respect to η_ϕ and η_A .

C. Networks with Physical IRSs

In purely simulated environments, ZoSGA outperforms TTS-SSCO, so much so that we may claim it to be a new SOTA for IRS-aided sumrate optimization. Nonetheless, we would also like to evaluate its robustness in a practical setting with *physically modeled* IRSs. To that end, we first define the IRSs using a practically feasible Transmission Line (TL) equivalent of an electromagnetic (EM) model, as presented in [66]. This TL model accounts for the geometrical and electrical properties of the IRS elements, also referred to as patches. Specifically, this model takes into account reconfigurability, changes in response due to different angles of wave incidence, mutual coupling among closely spaced cells, and reflection losses.

An IRS can be classified as a spatially dispersive device, the reconfigurability of which is achieved by incorporating varactor diodes in its periodic structure. That is, the beamforming angles (of reflection) are controlled by changing DC voltages, thus tuning the capacitances of these diodes. Though there can be two scenarios when an EM wave impinges on an IRS surface,

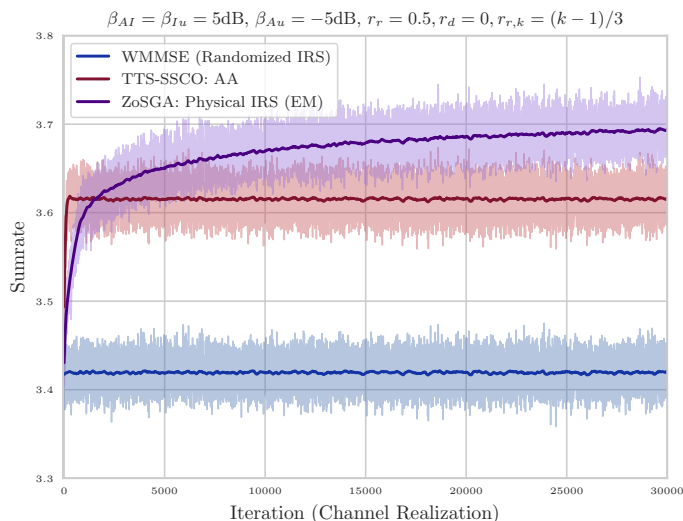


Fig. 7: Average system sumrates achieved by WMMSE [50] (with random IRS phase-shifts), TTS-SSCO [21] with a simulated IRS, and ZoSGA with a physical EM model of the IRS for the network in Figure 2.

namely, the traverse magnetic (TM) incidence and the traverse electric (TE) incidence, here we only consider the former for simplicity, mostly focusing on the empirical performance analysis. Moreover, on a side note, we employ the Floquet theorem (as assumed in [66]) so as to consider the periodic patches placed in an infinite array, with each element/patch behaving identically. Also, as per the same work, we consider three types of losses incurred in an IRS: Dielectric losses, ohmic losses, and losses due to active components.

Given a non-reconfigurable impedance surface, the TL model usually consists of a parallelly connected surface impedance of a reflective surface, Z_{surf} , and inductive impedance of the grounded dielectric slab (Z_d^{TM}). Then, the input impedance is $Z_v = Z_{surf} \parallel Z_d$. For an IRS, however, the Z_{surf} is further comprised of a parallel connection between the unloaded surface impedance of the patch array Z_{patch} and the lumped impedance of a varactor diode Z_{var} , which is represented as a series of a resistor, inductance and capacitance as

$$Z_{var} = R_{var} + j\omega L_{var} + j\frac{1}{\omega C_{var}},$$

where the inductance L_{var} depends on the size of the lumped component and must be included in the varactor model to take into account the self-resonance of the component. The resistance R_{var} is included to account for the losses of the varactor. The variable capacitance C_{var} of the diode is used to vary Z_{var} .

The other two impedances, i.e. Z_d and Z_{patch} , depend on the properties of the substrate, the dielectric, and the angle of incidence. A detailed description of these is provided in [66, Section 4]. Once all the considered impedances of a patch have been evaluated, its phase-shift coefficient $\theta(C_{var})$ is given by

$$\theta(C_{var}) = a(C_{var})e^{j\phi(C_{var})} = \frac{Z_v(C_{var}) - \zeta_0}{Z_v(C_{var}) + \zeta_0},$$

where ζ_0 is the free space impedance. Thus, by changing the varactor capacitance C_{var} , we can change the varactor impedance Z_{var} , which changes the surface impedance Z_{surf} , which, in

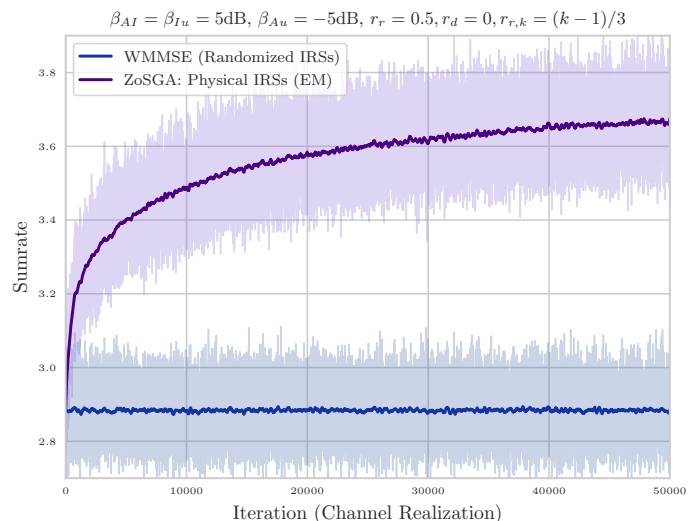


Fig. 8: Average system sumrates achieved by WMMSE [50] (with random IRS phase-shifts), and ZoSGA, with four Physical (EM model) IRSs as shown in the network in Figure 6.

turn, changes the input impedance of an IRS element Z_v , finally causing a change in the value of the phase-shift coefficient $\theta(C_{var})$. Due to our assumption that the Floquet theorem holds, this dependency flow is identical for all elements of an IRS. Thus, we may replicate this relation for all IRS elements, say q in number, and define a vector function $\theta(\cdot)$ of varactor capacitances $\mathbf{c}_{var} = [C_{var}^1 C_{var}^2 C_{var}^3 \dots C_{var}^q]^T$ as $\theta(\mathbf{c}_{var}) = [\theta(C_{var}^1) \theta(C_{var}^2) \theta(C_{var}^3) \dots \theta(C_{var}^q)]^T$.

Now that we have a model for a practical IRS, we would like to evaluate our first wireless network setting, with one IRS, to compare the relative performance drop, if any. As shown in Figure 7, the performance of the ZoSGA does drop when constrained in terms of the physical IRS model; this is very much expected, due to a decreased number of degrees of freedom in tuning the IRS parameters. However, the performance gain relative to the random phase-shifts is still substantial. More interestingly, ZoSGA outperforms TTS-SSCO –the latter optimizing both amplitudes and phases in an unconstrained manner– even in the presence of appreciable practical IRS constraints.

To complete our empirical study, which supports our claim of enabling totally model-free optimization of the IRS amplitudes and phase-shifts, we lastly consider an elaborate wireless network setting, as shown in Figure 6, consisting of two APs and four IRSs serving a total of eight users. We consider a MISO downlink scenario where a both APs transmit a common symbol to each user, i.e., the two APs are different only in their position in space. We consider the same channel model and network environment parameters as given in Subsections VI-A and VI-B, respectively. Then, the effective received channel by user k is expressed as

$$\mathbf{h}_k(\mathbf{C}_{var}, \omega) = \begin{bmatrix} \sum_{i=1}^2 \underbrace{\mathbf{G}_i^H \text{Diag}(\theta(\mathbf{c}_{var}^i)) \mathbf{h}_{r,k}^i}_{\theta_i\text{-non-LoS link}} + \underbrace{\mathbf{h}_{d,k,1}}_{\text{AP1 LoS link}} \\ \sum_{j=3}^4 \underbrace{\mathbf{G}_j^H \text{Diag}(\theta(\mathbf{c}_{var}^j)) \mathbf{h}_{r,k}^j}_{\theta_j\text{-non-LoS link}} + \underbrace{\mathbf{h}_{d,k,2}}_{\text{AP2 LoS link}} \end{bmatrix},$$

where the varactor capacitances of the i -th IRS are denoted by the vector \mathbf{c}_{var}^i , and where the matrix $\mathbf{C}_{var} = [c_{var}^1 c_{var}^2 c_{var}^3 c_{var}^4]$ combines all the varactor capacitances of the four IRSs. Using the

same learning rate scheme as above and a smoothing parameter $\mu = 10^{-12}$, we optimize the system sumrate using ZoSGA.

We averaged the results of 40 different simulations in Figure 8 to show not only the performance gain due to IRS capacitance tuning, but also the robustness of the approach under different realizations of the channels. The fact that the proposed approach is able to optimize a complicated network such as that in Figure 6, without any model information, verifies our claim of true model-free optimization capability of ZoSGA. We conjecture that the proposed optimization scheme can tackle a wide-range of problems arising in practical applications, with little to no additional input from the user.

VII. CONCLUSIONS

In this paper we introduced a zeroth-order stochastic gradient ascent (ZoSGA) method for the solution of two-stage stochastic programs with applications to model-free optimal beamforming for passive IRS-assisted stochastic network utility maximization. ZoSGA is amenable to rigorous convergence analysis and achieves state-of-the-art convergence rates under two general sets of assumptions, capturing a wide range of realistic scenarios. By specializing to the case of sumrate maximization, we numerically demonstrated that ZoSGA outperforms current state-of-the-art model-based methodologies on three distinct network settings, yielding solutions of substantially higher quality and in a computationally efficient manner, while evading practical limitations that are inherent to current methods. Our numerical results confirmed that ZoSGA learns (near-)optimal passive IRS beamformers based solely on conventional effective CSI and in absence of channel models and spatial network configuration information, also verifying our theoretical expectations.

REFERENCES

- [1] F. Guo, F. R. Yu, H. Zhang, X. Li, H. Ji, and V. C. Leung, "Enabling massive IoT toward 6G: A comprehensive survey," *IEEE Internet of Things J.*, vol. 8, no. 15, pp. 11891–11915, 2021.
- [2] W. Jiang, B. Han, M. A. Habibi, and H. D. Schotten, "The road towards 6G: A comprehensive survey," *IEEE Open J. Commun. Soc.*, vol. 2, pp. 334–366, 2021.
- [3] H. Tataria, M. Shafi, A. F. Molisch, M. Dohler, H. Sjöland, and F. Tufvesson, "6G wireless systems: Vision, requirements, challenges, insights, and opportunities," *Proc. IEEE*, vol. 109, no. 7, pp. 1166–1199, 2021.
- [4] X. You, C.-X. Wang, J. Huang, X. Gao, Z. Zhang, M. Wang, Y. Huang, C. Zhang, Y. Jiang, J. Wang, et al., "Towards 6G wireless communication networks: Vision, enabling technologies, and new paradigm shifts," *Sci. China Inf. Sci.*, vol. 64, pp. 1–74, 2021.
- [5] F. Liu, Y. Cui, C. Masouros, J. Xu, T. X. Han, Y. C. Eldar, and S. Buzzi, "Integrated sensing and communications: Towards dual-functional wireless networks for 6G and beyond," *IEEE J. Sel. Areas Commun.*, 2022.
- [6] E. G. Larsson, O. Edfors, F. Tufvesson, and T. L. Marzetta, "Massive MIMO for next generation wireless systems," *IEEE Commun. Mag.*, vol. 52, no. 2, pp. 186–195, 2014.
- [7] A. Gotsis, S. Stefanatos, and A. Alexiou, "UltraDense networks: The new wireless frontier for enabling 5G access," *IEEE Veh. Technol. Mag.*, vol. 11, no. 2, pp. 71–78, 2016.
- [8] J. G. Andrews, S. Buzzi, W. Choi, S. V. Hanly, A. Lozano, A. C. Soong, and J. C. Zhang, "What will 5G be?," *IEEE J. Sel. Areas Commun.*, vol. 32, no. 6, pp. 1065–1082, 2014.
- [9] M. Shafi, A. F. Molisch, P. J. Smith, T. Haustein, P. Zhu, P. De Silva, F. Tufvesson, A. Benjebbour, and G. Wunder, "5G: A tutorial overview of standards, trials, challenges, deployment, and practice," *IEEE J. Sel. Areas Commun.*, vol. 35, no. 6, pp. 1201–1221, 2017.
- [10] M. El-kashlan, T. Q. Duong, and H.-H. Chen, "Millimeter-wave communications for 5G: fundamentals: Part I [guest editorial]," *IEEE Commun. Mag.*, vol. 52, no. 9, pp. 52–54, 2014.
- [11] X. Wang, L. Kong, F. Kong, F. Qiu, M. Xia, S. Arnon, and G. Chen, "Millimeter wave communication: A comprehensive survey," *IEEE Commun. Surv. Tutor.*, vol. 20, no. 3, pp. 1616–1653, 2018.
- [12] F. Al-Ogaili and R. M. Shubair, "Millimeter-wave mobile communications for 5G: Challenges and opportunities," in *2016 IEEE Int. Symp. Antennas Propag. (APSURSI)*, 2016, pp. 1003–1004.
- [13] M. Kamel, W. Hamouda, and A. Youssef, "Ultra-dense networks: A survey," *IEEE Commun. Surv. Tutor.*, vol. 18, no. 4, pp. 2522–2545, 2016.
- [14] J. F. Valenzuela-Valdés, A. Palomares, J. C. González-Macías, A. Valenzuela-Valdés, P. Padilla, and F. Luna-Valero, "On the ultra-dense small cell deployment for 5G networks," in *2018 IEEE 5G World Forum (5GWF)*. IEEE, 2018, pp. 369–372.
- [15] D. F. Sievenpiper, J. H. Schaffner, H. J. Song, R. Y. Loo, and G. Tandonan, "Two-dimensional beam steering using an electrically tunable impedance surface," *IEEE Trans. Antennas Propag.*, vol. 51, no. 10, pp. 2713–2722, 2003.
- [16] S. V. Hum, M. Okoniewski, and R. J. Davies, "Realizing an electronically tunable reflectarray using varactor diode-tuned elements," *IEEE Microw. Wirel. Compon. Lett.*, vol. 15, no. 6, pp. 422–424, 2005.
- [17] H. Kamoda, T. Iwasaki, J. Tsumochi, T. Kuki, and O. Hashimoto, "60-GHz electronically reconfigurable large reflectarray using single-bit phase shifters," *IEEE Trans. Antennas Propag.*, vol. 59, no. 7, pp. 2524–2531, 2011.
- [18] J. Zhao, Q. Cheng, J. Chen, M. Q. Qi, W. X. Jiang, and T. J. Cui, "A tunable metamaterial absorber using varactor diodes," *New J. Phys.*, vol. 15, no. 4, pp. 043049, 2013.
- [19] A. Araghi, M. Khalily, M. Safaei, A. Bagheri, V. Singh, F. Wang, and R. Tafazolli, "Reconfigurable intelligent surface (RIS) in the sub-6 GHz band: Design, implementation, and real-world demonstration," *IEEE Access*, vol. 10, pp. 2646–2655, 2022.
- [20] H. Guo, Y.-C. Liang, J. Chen, and E. G. Larsson, "Weighted sum-rate maximization for reconfigurable intelligent surface aided wireless networks," *IEEE Trans. Wirel. Commun.*, vol. 19, no. 5, pp. 3064–3076, 2020.
- [21] M.-M. Zhao, Q. Wu, M.-J. Zhao, and R. Zhang, "Intelligent reflecting surface enhanced wireless networks: Two-timescale beamforming optimization," *IEEE Trans. Wirel. Commun.*, vol. 20, no. 1, pp. 2–17, 2020.
- [22] M.-M. Zhao, A. Liu, Y. Wan, and R. Zhang, "Two-timescale beamforming optimization for intelligent reflecting surface aided multiuser communication with QoS constraints," *IEEE Trans. Wirel. Commun.*, vol. 20, no. 9, pp. 6179–6194, 2021.
- [23] Z. Yang, M. Chen, W. Saad, W. Xu, M. Shikh-Bahaei, H. V. Poor, and S. Cui, "Energy-efficient wireless communications with distributed reconfigurable intelligent surfaces," *IEEE Trans. Wirel. Commun.*, vol. 21, no. 1, pp. 665–679, 2021.
- [24] B. Zheng, C. You, W. Mei, and R. Zhang, "A survey on channel estimation and practical passive beamforming design for intelligent reflecting surface aided wireless communications," *IEEE Commun. Surv. Tutor.*, vol. 24, no. 2, pp. 1035–1071, 2022.
- [25] M. Munochiveyi, A. C. Pogaku, D.-T. Do, A.-T. Le, M. Voznak, and N. D. Nguyen, "Reconfigurable intelligent surface aided multi-user communications: State-of-the-art techniques and open issues," *IEEE Access*, vol. 9, pp. 118584–118605, 2021.
- [26] Q. Wu and R. Zhang, "Intelligent reflecting surface enhanced wireless network via joint active and passive beamforming," *IEEE Trans. Wirel. Commun.*, vol. 18, no. 11, pp. 5394–5409, 2019.
- [27] Q. Wu and R. Zhang, "Towards smart and reconfigurable environment: Intelligent reflecting surface aided wireless network," *IEEE Commun. Mag.*, vol. 58, no. 1, pp. 106–112, 2019.
- [28] K. Faisal and W. Choi, "Machine learning approaches for reconfigurable intelligent surfaces: a survey," *IEEE Access*, vol. 10, pp. 27343–27367, 2022.
- [29] M. Hong, Q. Li, and Y.-F. Liu, "Decomposition by successive convex approximation: A unifying approach for linear transceiver design in heterogeneous networks," *IEEE Trans. Wirel. Commun.*, vol. 15, no. 2, pp. 1377–1392, 2015.
- [30] G. Scutari, F. Facchinei, P. Song, D. P. Palomar, and J.-S. Pang, "Decomposition by partial linearization: Parallel optimization of multi-agent systems," *IEEE Trans. Signal Process.*, vol. 62, no. 3, pp. 641–656, 2013.
- [31] Y. Yang, G. Scutari, D. P. Palomar, and M. Pesavento, "A parallel decomposition method for nonconvex stochastic multi-agent optimization problems," *IEEE Trans. Signal Process.*, vol. 64, no. 11, pp. 2949–2964, 2016.
- [32] M. Jian and Y. Zhao, "A modified off-grid SBL channel estimation and transmission strategy for RIS-assisted wireless communication systems," in *2020 Int. Wirel. Commun. Mobile Comput. Conf. (IWCMC)*, 2020, pp. 1848–1853.

- [33] X. Chen, J. Shi, Z. Yang, and L. Wu, “Low-complexity channel estimation for intelligent reflecting surface-enhanced massive MIMO,” *IEEE Wirel. Commun. Lett.*, vol. 10, no. 5, pp. 996–1000, 2021.
- [34] Y. Lin, S. Jin, M. Matthaiou, and X. You, “Tensor-based algebraic channel estimation for hybrid IRS-assisted MIMO-OFDM,” *IEEE Trans. Wirel. Commun.*, vol. 20, no. 6, pp. 3770–3784, 2021.
- [35] A. L. Swindlehurst, G. Zhou, R. Liu, C. Pan, and M. Li, “Channel estimation with reconfigurable intelligent surfaces—A general framework,” *Proc. IEEE*, vol. 110, no. 9, pp. 1312–1338, 2022.
- [36] A. Taha, M. Alrabeiah, and A. Alkhateeb, “Deep learning for large intelligent surfaces in millimeter wave and massive MIMO systems,” in *2019 IEEE Global Commun. Conf. (GLOBECOM)*, 2019, pp. 1–6.
- [37] E. Balevi, A. Doshi, A. Jalal, A. Dimakis, and J. G. Andrews, “High dimensional channel estimation using deep generative networks,” *IEEE J. Sel. Areas Commun.*, vol. 39, no. 1, pp. 18–30, 2020.
- [38] B. Yang, X. Cao, C. Huang, C. Yuen, L. Qian, and M. Di Renzo, “Intelligent spectrum learning for wireless networks with reconfigurable intelligent surfaces,” *IEEE Trans. Veh. Technol.*, vol. 70, no. 4, pp. 3920–3925, 2021.
- [39] S. Zhang, S. Zhang, F. Gao, J. Ma, and O. A. Dobre, “Deep learning optimized sparse antenna activation for reconfigurable intelligent surface assisted communication,” *IEEE Trans. Commun.*, vol. 69, no. 10, pp. 6691–6705, 2021.
- [40] F. B. Mismar, B. L. Evans, and A. Alkhateeb, “Deep reinforcement learning for 5g networks: Joint beamforming, power control, and interference coordination,” *IEEE Trans. Commun.*, vol. 68, no. 3, pp. 1581–1592, 2019.
- [41] A. Taha, Y. Zhang, F. B. Mismar, and A. Alkhateeb, “Deep reinforcement learning for intelligent reflecting surfaces: Towards standalone operation,” in *2020 IEEE 21st Int. Workshop Signal Process. Adv. Wirel. Commun. (SPAWC)*, 2020, pp. 1–5.
- [42] H. Yang, Z. Xiong, J. Zhao, D. Niyato, L. Xiao, and Q. Wu, “Deep reinforcement learning-based intelligent reflecting surface for secure wireless communications,” *IEEE Trans. Wirel. Commun.*, vol. 20, no. 1, pp. 375–388, 2020.
- [43] G. Lee, M. Jung, A. T. Z. Kasgari, W. Saad, and M. Bennis, “Deep reinforcement learning for energy-efficient networking with reconfigurable intelligent surfaces,” in *2020 IEEE Int. Conf. Commun. (ICC)*, 2020, pp. 1–6.
- [44] C. Huang, R. Mo, and C. Yuen, “Reconfigurable intelligent surface assisted multiuser MISO systems exploiting deep reinforcement learning,” *IEEE J. Sel. Areas Commun.*, vol. 38, no. 8, pp. 1839–1850, 2020.
- [45] Z. Yang, Y. Liu, Y. Chen, and J. T. Zhou, “Deep reinforcement learning for RIS-aided non-orthogonal multiple access downlink networks,” in *2020 IEEE Global Commun. Conf. (GLOBECOM)*, IEEE, 2020, pp. 1–6.
- [46] X. Xie, S. Jiao, and Z. Ding, “A reinforcement learning approach for an IRS-assisted noma network,” *arXiv:2106.09611*, 2021.
- [47] S. Evmorfos, A. P. Petropulu, and H. V. Poor, “Deep reinforcement learning for IRS phase shift design in spatiotemporally correlated environments,” *arXiv:2211.09726*, 2022.
- [48] T. P. Lillicrap, J. J. Hunt, A. Pritzel, N. Heess, T. Erez, Y. Tassa, D. Silver, and D. Wierstra, “Continuous control with deep reinforcement learning,” *arXiv:1509.02971*, 2015.
- [49] Y. Liu, Q. Hu, Y. Cai, G. Yu, and G. Y. Li, “Deep-unfolding beamforming for intelligent reflecting surface assisted full-duplex systems,” *IEEE Trans. Wirel. Commun.*, 2021.
- [50] Q. Shi, M. Razaviyayn, Z. Q. Luo, and C. He, “An iteratively weighted MMSE approach to distributed sum-utility maximization for a MIMO interfering broadcast channel,” *IEEE Trans. Signal Process.*, vol. 59, pp. 4331–4340, 2011.
- [51] S. Dempe, *Bilevel Programming: Implicit Function Approach*, pp. 260–266, Springer US, Boston, MA, 2009.
- [52] K. Kreutz-Delgado, “The complex gradient operator and the $\mathbb{C}\mathbb{R}$ -calculus,” *arXiv:0906.4835*, 2009.
- [53] A. L. Dontchev and R. T. Rockafellar, *Implicit Functions and Solution Mappings*, Springer Monogr. in Math. Springer New York, NY, 2009.
- [54] P. Bernhard and A. Rapaport, “On a theorem of Danskin with an application to a theorem of Von Neumann-Sion,” *Nonlinear Anal. Theory Methods Appl.*, vol. 24, no. 8, pp. 1163–1181, 1995.
- [55] D. Davis and D. Drusvyatskiy, “Stochastic model-based minimization of weakly convex functions,” *SIAM J. Optim.*, vol. 29, no. 1, pp. 207–239, 2019.
- [56] A. Shapiro, D. Dentcheva, and A. Ruszczyński, *Lectures on Stochastic Programming: Modeling and Theory*, MOS-SIAM Ser. Optim. SIAM & Mathematical Optimization Society, Philadelphia, 2014.
- [57] D. S. Kalogerias and W. B. Powell, “Zeroth-order stochastic compositional algorithms for risk-aware learning,” *SIAM J. Optim.*, vol. 32, no. 2, pp. 386–416, 2022.
- [58] Y. Nesterov and V. Spokoiny, “Random gradient-free minimization of convex functions,” *Found. Comput. Math.*, vol. 17, pp. 527–566, 2017.
- [59] S. Pougkakiotis and D. S. Kalogerias, “A zeroth-order proximal stochastic gradient method for weakly convex stochastic optimization,” *arXiv:2205.01633*, 2022.
- [60] H. Kumar, D. S. Kalogerias, G. J. Pappas, and A. Ribeiro, “Zeroth-order deterministic policy gradient,” *arXiv:2006.07314*, 2020.
- [61] A. Savitzky and M. J. Golay, “Smoothing and differentiation of data by simplified least squares procedures,” *Analytical chemistry*, vol. 36, no. 8, pp. 1627–1639, 1964.
- [62] M. R. McKay and I. B. Collings, “General capacity bounds for spatially correlated rician MIMO channels,” *IEEE Trans. Inf. Theory*, vol. 51, no. 9, pp. 3121–3145, 2005.
- [63] S. Loyka, “Channel capacity of MIMO architecture using the exponential correlation matrix,” *IEEE Commun. Lett.*, vol. 5, no. 9, pp. 369–371, 2001.
- [64] J. Choi and D. J. Love, “Bounds on eigenvalues of a spatial correlation matrix,” *IEEE Commun. Lett.*, vol. 18, no. 8, pp. 1391–1394, 2014.
- [65] Q. Wu and R. Zhang, “Intelligent reflecting surface enhanced wireless network via joint active and passive beamforming,” *IEEE Trans. Wirel. Commun.*, vol. 18, no. 11, pp. 5394–5409, 2019.
- [66] F. Costa and M. Borgese, “Electromagnetic model of reflective intelligent surfaces,” *IEEE Open J. Commun. Soc.*, vol. 2, pp. 1577–1589, 2021.
- [67] H. Yin, D. Gesbert, M. Filippou, and Y. Liu, “A coordinated approach to channel estimation in large-scale multiple-antenna systems,” *IEEE J. Sel. Areas Commun.*, vol. 31, no. 2, pp. 264–273, 2013.